

Chapter 8

Surface Morphology and Structure

8.1 The Application of VSI (Vertical Scanning Interferometry) to the Study of Crystal Surface Processes¹

8.1.1 Introduction

The processes which occur at the surfaces of crystals depend on many external and internal factors such as crystal structure and composition, conditions of a medium where the crystal surface exists and others. The appearance of a crystal surface is the result of complexity of interactions between the crystal surface and the environment. The mechanisms of surface processes such as dissolution or growth are studied by the physical chemistry of surfaces. There are a lot of computational techniques which allows us to predict the changing of surface morphology of different minerals which are influenced by different conditions such as temperature, pressure, pH and chemical composition of solution reacting with the surface. For example, Monte Carlo method is widely used to simulate the dissolution or growth of crystals. However, the theoretical models of surface processes need to be verified by natural observations. We can extract a lot of useful information about the surface processes through studying the changing of crystal surface structure under influence of environmental conditions. The changes in surface structure can be studied through the observation of crystal surface topography. The topography can be directly observed macroscopically or by using microscopic techniques. Microscopic observation allows us to study even very small changes and estimate the rate of processes by observing changing the crystal surface topography in time.

Much laboratory worked under the reconstruction of surface changes and interpretation of dissolution and precipitation kinetics of crystals. Invention of AFM made possible to monitor changes of surface structure during dissolution or growth. However, to detect and quantify the results of dissolution processes or growth it is necessary to determine surface area changes over a significantly larger field of view than AFM can provide. More recently, vertical scanning interferometry (VSI) has been developed as new tool to distinguish and trace the reactive parts of crystal surfaces. VSI and AFM are complementary techniques and practically well suited to detect surface changes.

VSI technique provides a method for quantification of surface topography at the angstrom to nanometer level. Time-dependent VSI measurements can be used to study the surface-normal retreat across crystal and other solid surfaces during dissolution process. Therefore, VSI can be used to directly and nondirectly measure mineral dissolution rates with high precision. Analogically, VSI can be used to study kinetics of crystal growth.

¹This content is available online at <<http://cnx.org/content/m22326/1.4/>>.

8.1.2 Physical principles of optical interferometry

Optical interferometry allows us to make extremely accurate measurements and has been used as a laboratory technique for almost a hundred years. Thomas Young observed interference of light and measured the wavelength of light in an experiment, performed around 1801. This experiment gave an evidence of Young's arguments for the wave model for light. The discovery of interference gave a basis to development of interferometry techniques widely successfully used as in microscopic investigations, as in astronomic investigations.

The physical principles of optical interferometry exploit the wave properties of light. Light can be thought as electromagnetic wave propagating through space. If we assume that we are dealing with a linearly polarized wave propagating in a vacuum in z direction, electric field E can be represented by a sinusoidal function of distance and time.

$$E(x, y, z, t) = a \cos [2\pi (vt - z/\lambda)] \quad (8.1)$$

Where a is the amplitude of the light wave, v is the frequency, and λ is its wavelength. The term within the square brackets is called the phase of the wave. Let's rewrite this equation in more compact form,

$$E(x, y, z, t) = a \cos [\omega t - kz] \quad (8.2)$$

where $\omega = 2\pi v$ is the circular frequency, and $k = 2\pi/\lambda$ is the propagation constant. Let's also transform this second equation into a complex exponential form,

$$E(x, y, z, t) = \text{Re}\{a \exp(i\varphi) \exp(i\omega t)\} = \text{Re}\{A \exp(i\omega t)\} \quad (8.3)$$

where $\varphi = 2\pi z/\lambda$ and $A = \exp(-i\varphi)$ is known as the complex amplitude. If n is a refractive index of a medium where the light propagates, the light wave traverses a distance d in such a medium. The equivalent optical path in this case is

$$p = n \cdot d \quad (8.4)$$

When two light waves are superposed, the result intensity at any point depends on whether reinforce or cancel each other (Figure 8.1). This is well known phenomenon of interference. We will assume that two waves are propagating in the same direction and are polarized with their field vectors in the same plane. We will also assume that they have the same frequency. The complex amplitude at any point in the interference pattern is then the sum of the complex amplitudes of the two waves, so that we can write,

$$A = A_1 + A_2 \quad (8.5)$$

where $A_1 = a_1 \exp(-i\varphi_1)$ and $A_2 = a_2 \exp(-i\varphi_2)$ are the complex amplitudes of two waves. The resultant intensity is, therefore,

$$I = |A|^2 = I_1 + I_2 + 2(I_1 I_2)^{1/2} \cos \Delta\varphi \quad (8.6)$$

where I_1 and I_2 are the intensities of two waves acting separately, and $\Delta\varphi = \varphi_1 - \varphi_2$ is the phase difference between them. If the two waves are derived from a common source, the phase difference corresponds to an optical path difference,

$$\Delta p = (\lambda/2\pi) \Delta\varphi \quad (8.7)$$

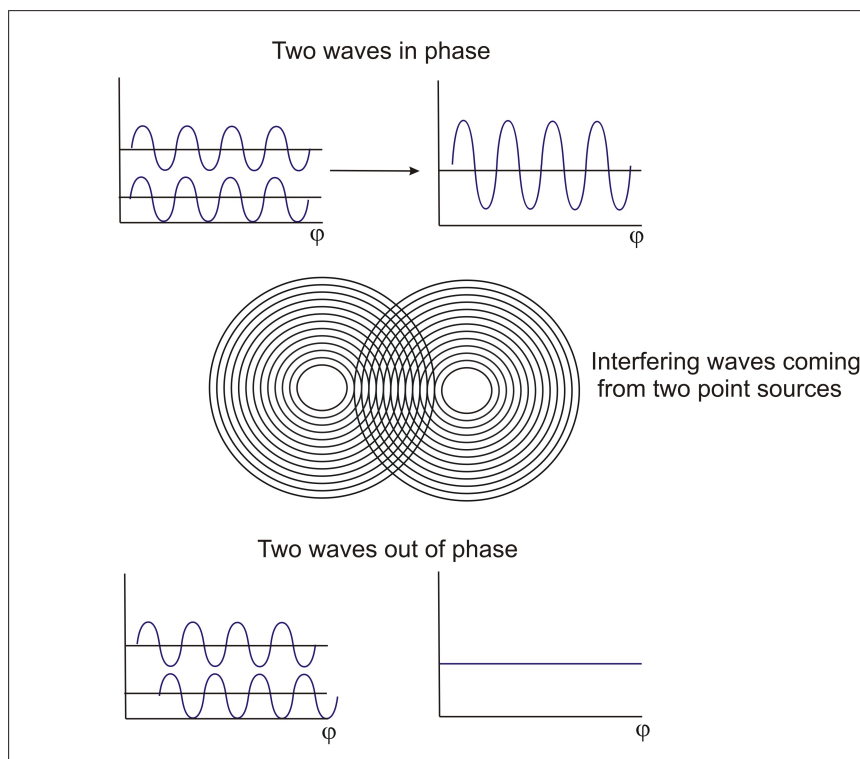


Figure 8.1: The scheme of interferometric wave interaction when two waves interact with each other, the amplitude of resulting wave will increase or decrease. The value of this amplitude depends on phase difference between two original waves.

If $\Delta\phi$, the phase difference between the beams, varies linearly across the field of view, the intensity varies sinusoidally, giving rise to alternating light and dark bands or fringes (Figure 8.1). The intensity in an interference pattern has its maximum value

$$I_{\max} = I_1 + I_2 + 2(I_1 I_2)^{1/2} \quad (8.8)$$

when $\Delta\phi = 2m\pi$, where m is an integer and its minimum value

$$I_{\min} = I_1 + I_2 - 2(I_1 I_2)^{1/2} \quad (8.9)$$

when $\Delta\phi = (2m + 1)\pi$.

The principle of interferometry is widely used to develop many types of interferometric set ups. One of the earliest set ups is Michelson interferometry. The idea of this interferometry is quite simple: interference fringes are produced by splitting a beam of monochromatic light so that one beam strikes a fixed mirror and the other a movable mirror. An interference pattern results when the reflected beams are brought back together. The Michelson interferometric scheme is shown in Figure 8.2.

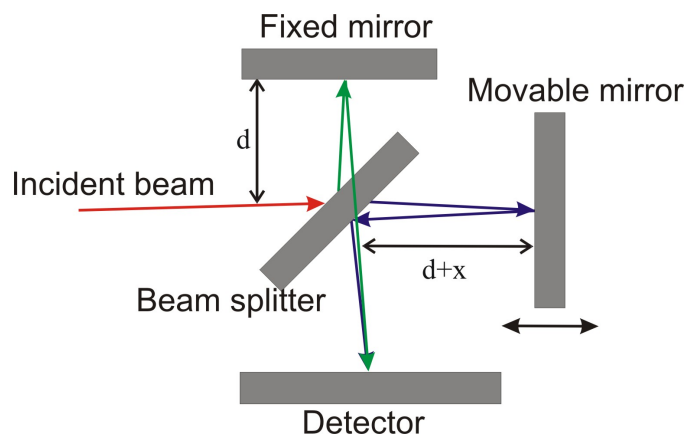


Figure 8.2: Schematic representation of a Michelson interferometry set-up.

The difference of path lengths between two beams is $2x$ because beams traverse the designated distances twice. The interference occurs when the path difference is equal to integer numbers of wavelengths,

$$\Delta p = 2x = m\lambda, m = 0, \pm 1, \pm 2 \dots \quad (8.10)$$

Modern interferometric systems are more complicated. Using special phase-measurement techniques they are capable of performing much more accurate height measurements than can be obtained just by directly looking at the interference fringes and measuring how they depart from being straight and equally spaced. Typically an interferometric system consists of a light source, beamsplitter, objective system, system of registration of signals, and transformation into digital format and a computer which processes the data. Vertical scanning interferometry contains all these parts. Figure 8.3 shows a configuration of a VSI interferometric system.

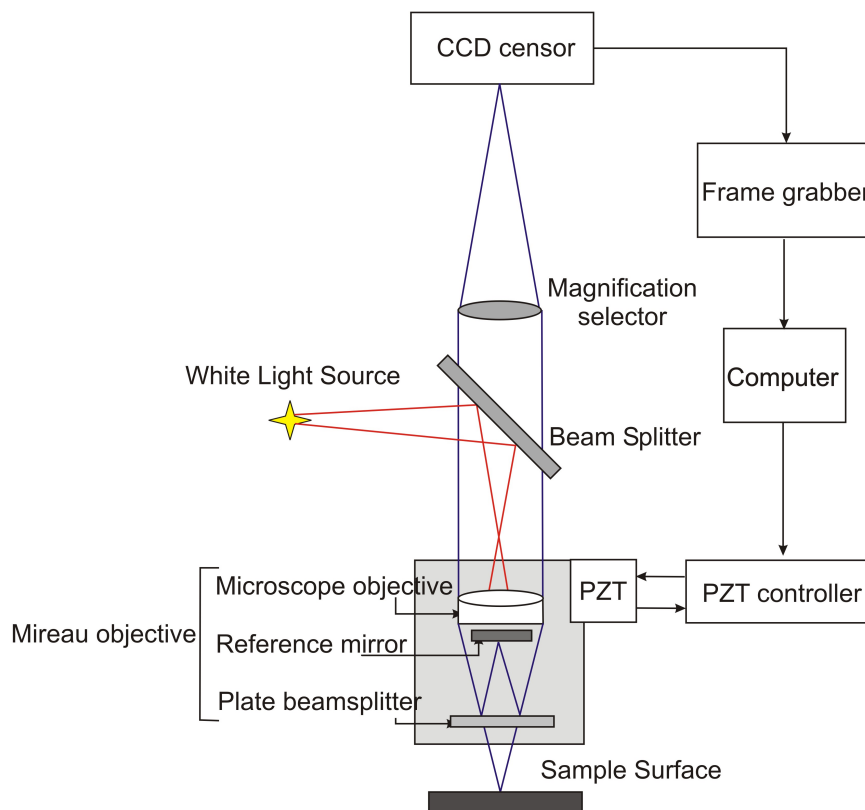


Figure 8.3: Schematic representation of the Vertical scanning interferometry (VSI) system.

Many of modern interferometric systems use Mirau objective in their constructions. Mirau objective is based on a Michelson interferometer. This objective consists of a lens, a reference mirror and a beamsplitter. The idea of getting interfering beams is simple: two beams (red lines) travel along the optical axis. Then they are reflected from the reference surface and the sample surface respectively (blue lines). After this these beams are recombined to interfere with each other. An illumination or light source system is used to direct light onto a sample surface through a cube beam splitter and the Mirau objective. The sample surface within the field of view of the objective is uniformly illuminated by those beams with different incidence angles. Any point on the sample surface can reflect those incident beams in the form of divergent cone. Similarly, the point on the reference symmetrical with that on the sample surface also reflects those illuminated beams in the same form.

The Mirau objective directs the beams reflected of the reference and the sample surface onto a CCD (charge-coupled device) sensor through a tube lens. The CCD sensor is an analog shift register that enables the transportation of analog signals (electric charges) through successive stages (capacitors), controlled by a clock signal. The resulting interference fringe pattern is detected by CCD sensor and the corresponding signal is digitized by a frame grabber for further processing with a computer.

The distance between a minimum and a maximum of the interferogram produced by two beams reflected from the reference and sample surface is known. That is, exactly half the wavelength of the light source. Therefore, with a simple interferogram the vertical resolution of the technique would be also limited to $\lambda/2$. If we will use a laser light as a light source with a wavelength of 300 nm the resolution would be only 150

nm. This resolution is not good enough for a detailed near-atomic scale investigation of crystal surfaces. Fortunately, the vertical resolution of the technique can be improved significantly by moving either the reference or the sample by a fraction of the wavelength of the light. In this way, several interferograms are produced. Then they are all overlaid, and their phase shifts compared by the computer software Figure 8.4. This method is widely known as phase shift interferometry (PSI).

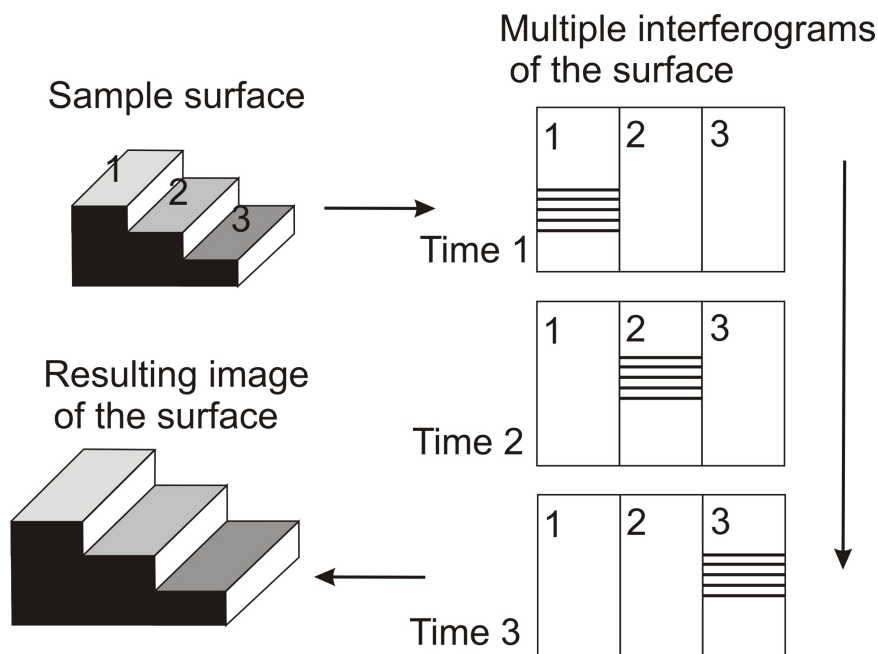


Figure 8.4: Sketch illustrating phase-shift technology. The sample is continuously moved along the vertical axes in order to scan surface topography. All interferograms are automatically overlaid using computer software.

Most optical testing interferometers now use phase-shifting techniques not only because of high resolution but also because phase-shifting is a high accuracy rapid way of getting the interferogram information into the computer. Also usage of this technique makes the inherent noise in the data taking process very low. As the result in a good environment angstrom or sub-angstrom surface height measurements can be performed. As it was said above, in phase-shifting interferometry the phase difference between the interfering beams is changed at a constant rate as the detector is read out. Once the phase is determined across the interference field, the corresponding height distribution on the sample surface can be determined. The phase distribution $\phi(x, y)$ is recorded by using the CCD camera.

Let's assign $A(x, y)$, $B(x, y)$, $C(x, y)$ and $D(x, y)$ to the resulting interference light intensities which are corresponded to phase-shifting steps of 0 , $\pi/2$, π and $3\pi/2$. These intensities can be obtained by moving the reference mirror through displacements of $\lambda/8$, $\lambda/4$ and $3\lambda/8$, respectively. The equations for the resulting intensities would be:

$$A(x, y) = I_1(x, y) + I_2(x, y) \cos \alpha(x, y) \quad (8.11)$$

$$B(x, y) = I_1(x, y) - I_2(x, y) \sin \alpha(x, y) \quad (8.12)$$

$$C(x, y) = I_1(x, y) - I_2(x, y) \cos\alpha(x, y) \quad (8.13)$$

$$D(x, y) = I_1(x, y) + I_2(x, y) \sin\alpha(x, y) \quad (8.14)$$

where $I_1(x, y)$ and $I_2(x, y)$ are two overlapping beams from two symmetric points on the test surface and the reference respectively. Solving equations (8.11)–(8.14), the phase map $\phi(x, y)$ of a sample surface will be given by the relation:

$$\varphi(x, y) = \frac{B(x, y) - D(x, y)}{A(x, y) - C(x, y)} \quad (8.15)$$

Once the phase is determined across the interference field pixel by pixel on a two-dimensional CCD array, the local height distribution/contour, $h(x, y)$, on the test surface is given by

$$h(x, y) = \frac{\lambda}{4\pi} \varphi(x, y) \quad (8.16)$$

Normally the resulted fringe can be in the form of a linear fringe pattern by adjusting the relative position between the reference mirror and sample surfaces. Hence any distorted interference fringe would indicate a local profile/contour of the test surface.

It is important to note that the Mireau objective is mounted on a capacitive closed-loop controlled PZT (piezoelectric actuator) as to enable phase shifting to be accurately implemented. The PZT is based on piezoelectric effect referred to the electric potential generated by applying pressure to piezoelectric material. This type of materials is used to convert electrical energy to mechanical energy and vice-versa. The precise motion that results when an electric potential is applied to a piezoelectric material has an importance for nanopositioning. Actuators using the piezo effect have been commercially available for 35 years and in that time have transformed the world of precision positioning and motion control.

Vertical scanning interferometer also has another name; white-light interferometry (WLI) because of using the white light as a source of light. With this type of source a separate fringe system is produced for each wavelength, and the resultant intensity at any point of examined surface is obtained by summing these individual patterns. Due to the broad bandwidth of the source the coherent length L of the source is short:

$$L = \frac{\lambda^2}{n\Delta\lambda} \quad (8.17)$$

where λ is the center wavelength, n is the refractive index of the medium, $\Delta\lambda$ is the spectral width of the source. In this way good contrast fringes can be obtained only when the lengths of interfering beams pathways are closed to each other. If we will vary the length of a pathway of a beam reflected from sample, the height of a sample can be determined by looking at the position for which a fringe contrast is a maximum. In this case interference pattern exist only over a very shallow depth of the surface. When we vary a pathway of sample-reflected beam we also move the sample in a vertical direction in order to get the phase at which maximum intensity of fringes will be achieved. This phase will be converted in height of a point at the sample surface.

The combination of phase shift technology with white-light source provides a very powerful tool to measure the topography of quite rough surfaces with the amplitude in heights about and the precision up to 1-2 nm. Through a developed software package for quantitatively evaluating the resulting interferogram, the proposed system can retrieve the surface profile and topography of the sample objects Figure 8.5.

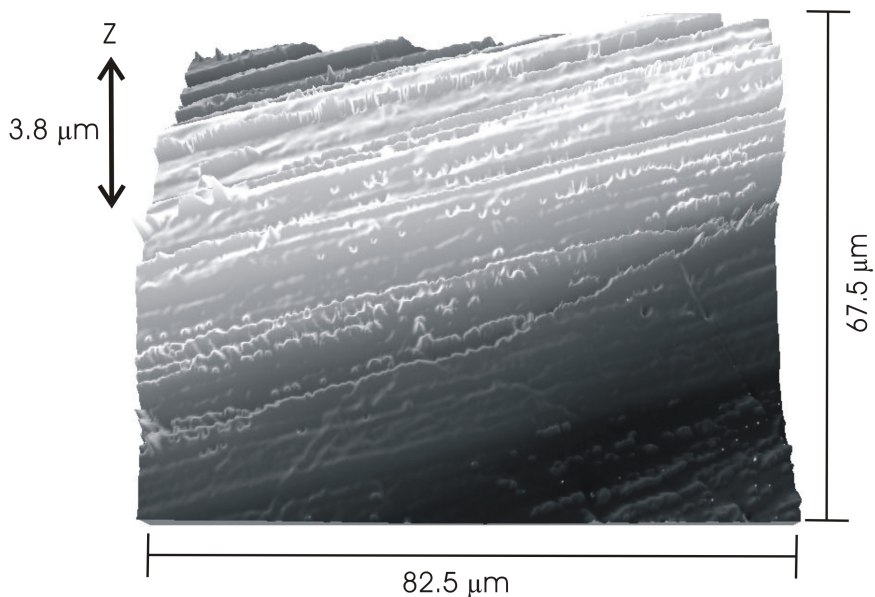


Figure 8.5: Example of muscovite surface topography, obtained by using VSI- 50x objective.

8.1.3 A comparison of common methods to determine surface topography: SEM, AFM and VSI

Except the interferometric methods described above, there are a several other microscopic techniques for studying crystal surface topography. The most common are scanning electron microscopy (SEM) and atomic force microscopy (AFM). All these techniques are used to obtain information about the surface structure. However they differ from each other by the physical principles on which they based.

8.1.3.1 Scanning electron microscopy

SEM allows us to obtain images of surface topography with the resolution much higher than the conventional light microscopes do. Also it is able to provide information about other surface characteristics such as chemical composition, electrical conductivity etc, see Figure 8.6. All types of data are generated by the reflecting of accelerated electron beams from the sample surface. When electrons strike the sample surface, they lose their energy by repeated random scattering and adsorption within an outer layer into the depth varying from 100 nm to 5 microns.

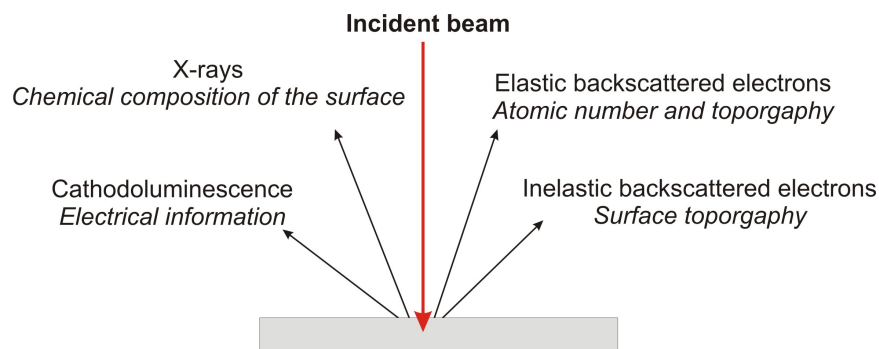


Figure 8.6: Scheme of electron beam-sample interaction at SEM analysis

The thickness of this outer layer also known as interactive layer depends on energy of electrons in the beam, composition and density of a sample. Result of the interaction between electron beam and the surface provides several types of signals. The main type is secondary or inelastic scattered electrons. They are produced as a result of interaction between the beam of electrons and weakly bound electrons in the conduction band of the sample. Secondary electrons are ejected from the k -orbitals of atoms within the surface layer of thickness about a few nanometers. This is because secondary electrons are low energy electrons (<50 eV), so only those formed within the first few nanometers of the sample surface have enough energy to escape and be detected. Secondary backscattered electrons provide the most common signal to investigate surface topography with lateral resolution up to 0.4 - 0.7 nm.

High energy beam electrons are elastic scattered back from the surface. This type of signal gives information about chemical composition of the surface because the energy of backscattered electrons depends on the weight of atoms within the interaction layer. Also this type of electrons can form secondary electrons and escape from the surface or travel farther into the sample than the secondary. The SEM image formed is the result of the intensity of the secondary electron emission from the sample at each x,y data point during the scanning of the surface.

8.1.3.2 Atomic force microscopy

AFM is a very popular tool to study surface dissolution. AFM set up consists of scanning a sharp tip on the end of a flexible cantilever which moves across a sample surface. The tips typically have an end radius of 2 to 20 nm, depending on tip type. When the tip touches the surface the forces of these interactions lead to deflection of a cantilever. The interaction between tip and sample surface involves mechanical contact forces, van der Waals forces, capillary forces, chemical bonding, electrostatic forces, magnetic forces etc. The deflection of a cantilever is usually measured by reflecting a laser beam off the back of the cantilever into a split photodiode detector. A schematic drawing of AFM can be seen in Figure 8.7. The two most commonly used modes of operation are contact mode AFM and tapping mode AFM, which are conducted in air or liquid environments.

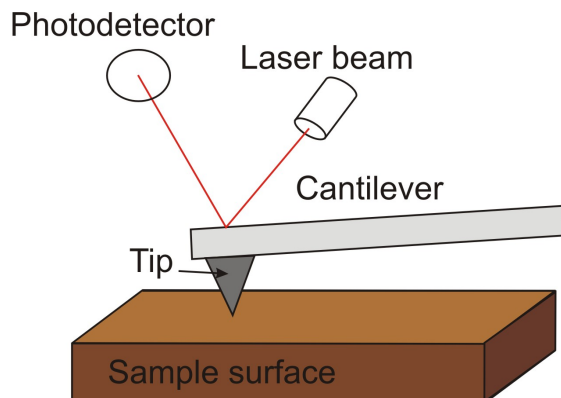


Figure 8.7: Schematic drawing of an AFM apparatus.

Working under the contact mode AFM scans the sample while monitoring the change in cantilever deflection with the split photodiode detector. Loop maintains a constant cantilever reflection by vertically moving the scanner to get a constant signal. The distance which the scanner goes by moving vertically at each x,y data point is stored by the computer to form the topographic image of the sample surface. Working under the tapping mode AFM oscillates the cantilever at its resonance frequency (typically ~ 300 kHz) and lightly “taps” the tip on the surface during scanning. The electrostatic forces increase when tip gets close to the sample surface, therefore the amplitude of the oscillation decreases. The laser deflection method is used to detect the amplitude of cantilever oscillation. Similar to the contact mode, feedback loop maintains a constant oscillation amplitude by moving the scanner vertically at every x,y data point. Recording this movement forms the topographical image. The advantage of tapping mode over contact mode is that it eliminates the lateral, shear forces present in contact mode. This enables tapping mode to image soft, fragile, and adhesive surfaces without damaging them while work under contact mode allows the damage to occur.

8.1.3.3 Comparison of techniques

All techniques described above are widely used in studying of surface nano- and micromorphology. However, each method has its own limitations and the proper choice of analytical technique depends on features of analyzed surface and primary goals of research.

All these techniques are capable to obtain an image of a sample surface with quite good resolution. The lateral resolution of VSI is much less, then for other techniques: 150 nm for VSI and 0.5 nm for AFM and SEM. Vertical resolution of AFM (0.5 Å) is better then for VSI (1 - 2 nm), however VSI is capable to measure a high vertical range of heights (1 mm) which makes possible to study even very rough surfaces. On the contrary, AFM allows us to measure only quite smooth surfaces because of its relatively small vertical scan range (7 μm). SEM has less resolution, than AFM because it requires coating of a conductive material with the thickness within several nm.

The significant advantage of VSI is that it can provide a large field of view (845 \times 630 μm for 10x objective) of tested surfaces. Recent studies of surface roughness characteristics showed that the surface roughness parameters increase with the increasing field of view until a critical size of 250,000 μm is reached. This value is larger then the maximum field of view produced by AFM (100 \times 100 μm) but can be easily obtained by VSI. SEM is also capable to produce images with large field of view. However, SEM is able to provide only 2D images from one scan while AFM and VSI let us to obtain 3D images. It makes quantitative

analysis of surface topography more complicated, for example, topography of membranes is studied by cross section and top view images.

	VSI	AFM	SEM
Lateral resolution	0.5-1.2 μm	0.5 nm	0.5-1 nm
Vertical resolution	2 nm	0.5 \AA	Only 2D images
Field of view	845 \times 630 μm (10x objective)	100 \times 100 μm	1-2 mm
Vertical range of scan	1 mm	10 μm	-
Preparation of a sample	-	-	Required coating of a conducted material
Required environment	Air	Air, liquid	Vacuum

Table 8.1: A comparison of VSI sample and resolution with AFM and SEM.

8.1.4 The experimental studying of surface processes using microscopic techniques

The limitations of each technique described above are critically important to choose appropriate technique for studying surface processes. Let's explore application of these techniques to study dissolution of crystals.

When crystalline matter dissolves the changes of the crystal surface topography can be observed by using microscopic techniques. If we will apply an unreactive mask (silicon for example) on crystal surface and place a crystalline sample into the experiment reactor then we get two types of surfaces: dissolving and remaining the same or unreacted. After some period of time the crystal surface starts to dissolve and change its z-level. In order to study these changes *ex situ* we can pull out a sample from the reaction cell then remove a mask and measure the average height difference $\Delta \bar{h}$ between the unreacted and dissolved areas. The average heights of dissolved and unreacted areas are obtained through digital processing of data obtained by microscopes. The velocity of normal surface retreat v_{SNR} during the time interval Δt is defined as

$$v_{\text{SNR}} = \frac{\Delta \bar{h}}{\Delta t}$$

Dividing this velocity by the molar volume \bar{V} (cm^3/mol) gives a global dissolution rate in the familiar units of moles per unit area per unit time:

$$R = \frac{v_{\text{SNR}}}{\bar{V}} \quad (8.18)$$

This method allows us to obtain experimental values of dissolution rates just by precise measuring of average surface heights. Moreover, using this method we can measure local dissolution rates at etch pits by monitoring changes in the volume and density of etch pits across the surface over time. VSI technique is capable to perform these measurements because of large vertical range of scanning. In order to get precise values of rates which are not depend on observing place of crystal surface we need to measure enough large areas. VSI technique provides data from areas which are large enough to study surfaces with heterogeneous dissolution dynamics and obtain average dissolution rates. Therefore, VSI makes possible to measure rates of normal surface retreat during the dissolution and observe formation, growth and distribution of etch pits on the surface.

However, if the mechanism of dissolution is controlled by dynamics of atomic steps and kink sites within a smooth atomic surface area, the observation of the dissolution process need to use a more precise technique. AFM is capable to provide information about changes in step morphology *in situ* when the dissolution

occurs. For example, immediate response of the dissolved surface to the changing of environmental conditions (concentrations of ions in the solution, pH etc.) can be studied by using AFM.

SEM is also used to examine micro and nanotexture of solid surfaces and study dissolution processes. This method allows us to observe large areas of crystal surface with high resolution which makes possible to measure a high variety of surfaces. The significant disadvantage of this method is the requirement to cover examine sample by conductive substance which limits the resolution of SEM. The other disadvantage of SEM is that the analysis is conducted in vacuum. Recent technique, environmental SEM or ESEM overcomes these requirements and makes possible even examine liquids and biological materials. The third disadvantage of this technique is that it produces only 2D images. This creates some difficulties to measure $\Delta\bar{h}$ within the dissolving area. One of advantages of this technique is that it is able to measure not only surface topography but also chemical composition and other surface characteristics of the surface. This fact is used to monitor changing in chemical composition during the dissolution.

8.1.5 Bibliography

- A. C. Lasaga, *Kinetic Theory in the Earth Sciences*. Princeton Univ. Press, Princeton, NJ (1998).
- A. Luttge, E. V. Bolton, and A. C. Lasaga A.C., *Am. J. Sci.*, 1999, **299**, 652.
- D. Kaczmarek, *Vacuum*, 2001, **62**, 303.
- P. Hariharan. *Optical interferometry*, Second edition, Academic press (2003) ISBN 0-12-311630-9.
- A. Luttge and P. G. Conrad, *Appl. Environ. Microbiol.*, 2004, **70**, 1627.
- A. C. Lasaga and A. Luttge, *American Mineralogist*, 2004, **89**, 527.
- K. J. Davis and A. Luttge, *Am. J. Sci.*, 2005, **305**, 727.
- S. H. Wang and Tay, *Meas. Sci. Technol.*, 2006, **17**, 617.
- A. Luttge and R. S. Arvidson, in *Kinetics of water-rock interaction*, Ed. S. Brantley, J. Kubicki, and A. White, Springer (2007).
- L. Zhang and A. Luttge, *American Mineralogist*, 2007, **92**, 1316.
- C. Fischer A. and Luttge, *Am. J. Sci.*, 2007, **307**, 955.
- Y. Wyart, G. Georges, C. Deumie, C. Amra, and P. Moulina, *J. Membrane Sci.*, 2008, **315**, 82.
- T. C. Vaimakis, E. D. Economou, and C. C. Trapalis, *J. Therm. Anal. Cal.*, 2008, **92**, 783.

8.2 AFM

8.2.1 Atomic Force Microscopy²

8.2.1.1 Introduction

Atomic force microscopy (AFM) is a high-resolution form of scanning probe microscopy, also known as scanning force microscopy (SFM). The instrument uses a cantilever with a sharp tip at the end to scan over the sample surface (Figure 8.8). As the probe scans over the sample surface, attractive or repulsive forces between the tip and sample, usually in the form of van der Waal forces but also can be a number of others such as electrostatic and hydrophobic/hydrophilic, cause a deflection of the cantilever. The deflection is measured by a laser (Figure 8.8) which is reflected off the cantilever into photodiodes. As one of the photodiodes collects more light, it creates an output signal that is processed and provides information about the vertical bending of the cantilever. This data is then sent to a scanner that controls the height of the probe as it moves across the surface. The variance in height applied by the scanner can then be used to produce a three-dimensional topographical representation of the sample.

²This content is available online at <<http://cnx.org/content/m34664/1.1/>>.

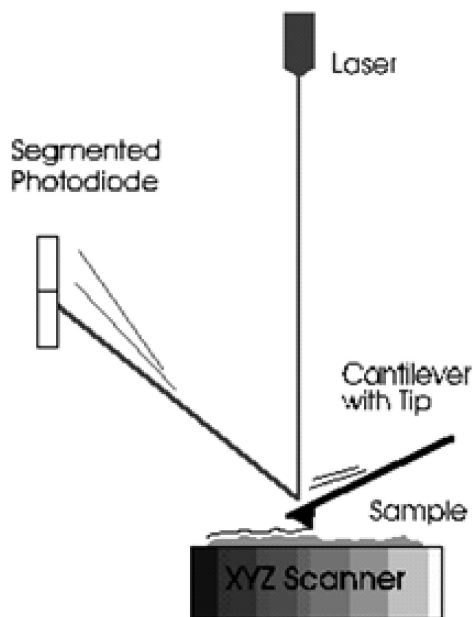


Figure 8.8: Simple schematic of atomic force microscope (AFM) apparatus. Adapted from H. G. Hansma, Department of Physics, University of California, Santa Barbara.

8.2.1.2 Modes of operation

8.2.1.2.1 Contact mode

The contact mode method utilizes a constant force for tip-sample interactions by maintaining a constant tip deflection (Figure 8.9). The tip communicates the nature of the interactions that the probe is having at the surface via feedback loops and the scanner moves the entire probe in order to maintain the original deflection of the cantilever. The constant force is calculated and maintained by using Hooke's Law, (8.19). This equation relates the force (F), spring constant (k), and cantilever deflection (x). Force constants typically range from 0.01 to 1.0 N/m. Contact mode usually has the fastest scanning times but can deform the sample surface. It is also only the only mode that can attain "atomic resolution."

$$F = -kx \tag{8.19}$$



Figure 8.9: Schematic diagram of probe and surface interaction in contact mode.

8.2.1.2.2 Tapping mode

In the tapping mode the cantilever is externally oscillated at its fundamental resonance frequency (Figure 8.10). A piezoelectric on top of the cantilever is used to adjust the amplitude of oscillation as the probe scans across the surface. The deviations in the oscillation frequency or amplitude due to interactions between the probe and surface are measured, and provide information about the surface or types of material present in the sample. This method is gentler than contact AFM since the tip is not dragged across the surface, but it does require longer scanning times. It also tends to provide higher lateral resolution than contact AFM.

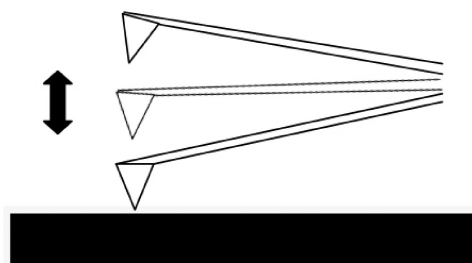


Figure 8.10: Diagram of probe and surface interaction in tapping mode.

8.2.1.2.3 Noncontact mode

For noncontact mode the cantilever is oscillated just above its resonance frequency and this frequency is decreased as the tip approaches the surface and experiences the forces associated with the material (Figure 8.11). The average tip-to-sample distance is measured as the oscillation frequency or amplitude is kept constant, which then can be used to image the surface. This method exerts very little force on the sample, which extends the lifetime of the tip. However, it usually does not provide very good resolution unless placed under a strong vacuum.

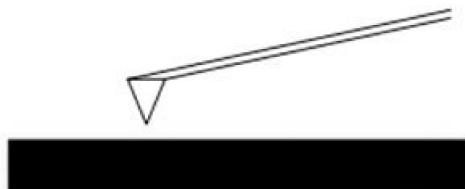


Figure 8.11: Diagram of probe and surface interaction in noncontact mode.

8.2.1.3 Experimental limitations

A common problem seen in AFM images is the presence of artifacts which are distortions of the actual topography, usually either due to issues with the probe, scanner, or image processing. The AFM scans slowly which makes it more susceptible to external temperature fluctuations leading to thermal drift. This leads to artifacts and inaccurate distances between topographical features.

It is also important to consider that the tip is not perfectly sharp and therefore may not provide the best aspect ratio, which leads to a convolution of the true topography. This leads to features appearing too large or too small since the width of the probe cannot precisely move around the particles and holes on the surface. It is for this reason that tips with smaller radii of curvature provide better resolution in imaging. The tip can also produce false images and poorly contrasted images if it is blunt or broken.

The movement of particles on the surface due to the movement of the cantilever can cause noise, which forms streaks or bands in the image. Artifacts can also be made by the tip being of inadequate proportions compared to the surface being scanned. It is for this reason that it is important to use the ideal probe for the particular application.

8.2.1.4 Sample size and preparation

The sample size varies with the instrument but a typical size is 8 mm by 8 mm with a typical height of 1 mm. Solid samples present a problem for AFM since the tip can shift the material as it scans the surface. Solutions or dispersions are best for applying as uniform of a layer of material as possible in order to get the most accurate value of particles' heights. This is usually done by spin-coating the solution onto freshly cleaved mica which allows the particles to stick to the surface once it has dried.

8.2.1.5 Applications of AFM

AFM is particularly versatile in its applications since it can be used in ambient temperatures and many different environments. It can be used in many different areas to analyze different kinds of samples such as semiconductors, polymers, nanoparticles, biotechnology, and cells amongst others. The most common application of AFM is for morphological studies in order to attain an understanding of the topography of the sample. Since it is common for the material to be in solution, AFM can also give the user an idea of the ability of the material to be dispersed as well as the homogeneity of the particles within that dispersion. It also can provide a lot of information about the particles being studied such as particle size, surface area, electrical properties, and chemical composition. Certain tips are capable of determining the principal mechanical, magnetic, and electrical properties of the material. For example, in magnetic force microscopy (MFM) the probe has a magnetic coating that senses magnetic, electrostatic, and atomic interactions with the surface. This type of scanning can be performed in static or dynamic mode and depicts the magnetic structure of the surface.

8.2.1.5.1 AFM of carbon nanotubes

Atomic force microscopy is usually used to study the topographical morphology of these materials. By measuring the thickness of the material it is possible to determine if bundling occurred and to what degree. Other dimensions of the sample can also be measured such as the length and width of the tubes or bundles. It is also possible to detect impurities, functional groups (Figure 8.12), or remaining catalyst by studying the images. Various methods of producing nanotubes have been found and each demonstrates a slightly different profile of homogeneity and purity. These impurities can be carbon coated metal, amorphous carbon, or other allotropes of carbon such as fullerenes and graphite. These facts can be utilized to compare the purity and homogeneity of the samples made from different processes, as well as monitor these characteristics as different steps or reactions are performed on the material. The distance between the tip and the surface has proven itself to be an important parameter in noncontact mode AFM and has shown that if the tip is moved past the threshold distance, approximately $30\ \mu\text{m}$, it can move or damage the nanotubes. If this occurs, a useful characterization cannot be performed due to these distortions of the image.

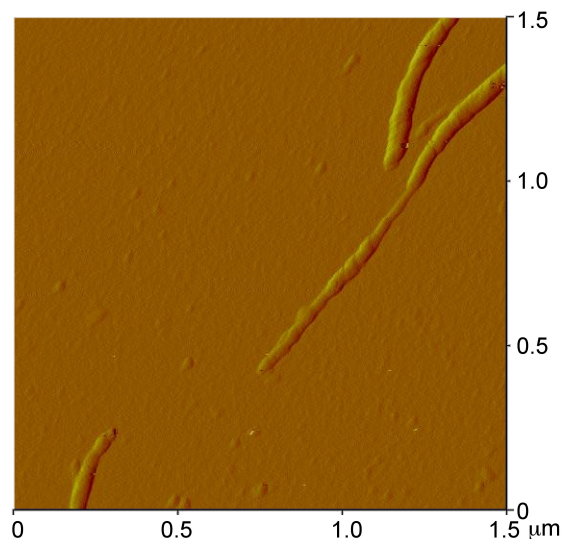


Figure 8.12: AFM image of a polyethyleneimine-functionalized single walled carbon nanotube (PEI-SWNT) showing the presence of PEI “globules” on the SWNT. Adapted from E. P. Dillon, C. A. Crouse, and A. R. Barron, *ACS Nano*, 2008, **2**, 156.

8.2.1.5.2 AFM of fullerenes

Atomic force microscopy is best applied to aggregates of fullerenes rather than individual ones. While the AFM can accurately perform height analysis of individual fullerene molecules, it has poor lateral resolution and it is difficult to accurately depict the width of an individual molecule. Another common issue that arises with contact AFM and fullerene deposited films is that the tip shifts clusters of fullerenes which can lead to discontinuities in sample images.

8.2.1.6 Bibliography

- R. Anderson and A. R. Barron, *J. Am. Chem. Soc.*, 2005, **127**, 10458.
- M. Bellucci, G. Gaggiotti, M. Marchetti, F. Micciulla, R. Mucciato, and M. Regi, *J. Physics: Conference Series*, 2007, **61**, 99.
- I. I. Bobrinetskii, V. N. Kukin, V. K. Nevolin, and M. M. Simunin. *Semiconductor*, 2008, **42**, 1496.
- S. H. Cohen and M. L. Lightbody. *Atomic Force Microscopy/Scanning Tunneling Microscopy 2*. Plenum, New York (1997).
- E. P. Dillon, C. A. Crouse, and A. R. Barron, *ACS Nano*, 2008, **2**, 156.
- C. Gu, C. Ray, S. Guo, and B. B. Akhremitchev, *J. Phys. Chem.*, 2007, **111**, 12898.
- G. Kaupp, *Atomic Force Microscopy, Scanning Nearfield Optical Microscopy and Nanoscratching: Application to Rough and Natural Surfaces*. Springer-Verlag, Berlin (2006).
- S. Morita, R. Wiesendanger, E. Meyer, and F. J. Giessibl. *Noncontact Atomic Force Microscopy*. Springer, Berlin (2002).

8.2.2 A Practical Guide to Using the Nanoscope Atomic Force Microscope³

The following is intended as a guide for use of the Nanoscope AFM system within the Shared Equipment Authority at Rice University (<http://sea.rice.edu>⁴). However, it can be adapted for similar AFM instruments.

NOTE: Please familiarize yourself with the Figures. All relevant parts of the AFM setup are shown.

8.2.2.1 Initial setup

Step 1. Sign in.

Step 2. Turn on each component shown in Figure 8.13.

- a. The controller that powers the scope (the switch is at the back of the box).
- b. The camera monitor.
- c. The white light source.

Step 3. Select imaging mode using the mode selector switch is located on the left hand side of the atomic force microscope (AFM) base (Figure 8.14), there are three modes:

- a. Scanning tunneling microscopy (STM).
- b. Atomic force microscopy/lateral force microscopy (AFM/LFM).
- c. Tapping mode atomic force microscopy (TM-AFM).

³This content is available online at <<http://cnx.org/content/m45758/1.1/>>.

⁴<http://sea.rice.edu/>

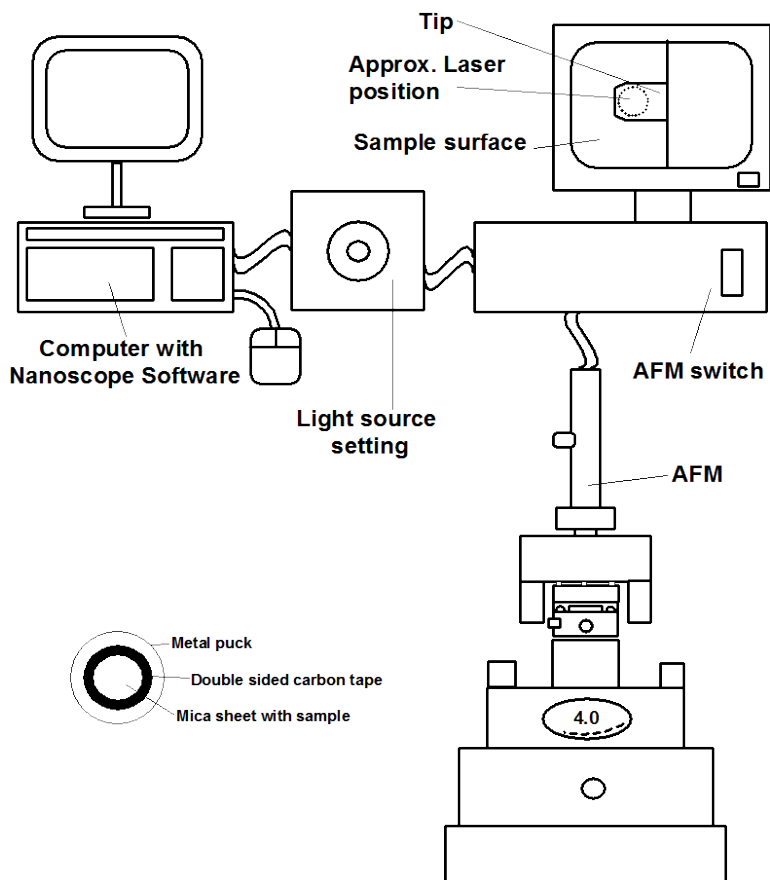


Figure 8.13: Schematic representation of the AFM computer, light source, camera set-up, and sample puck.

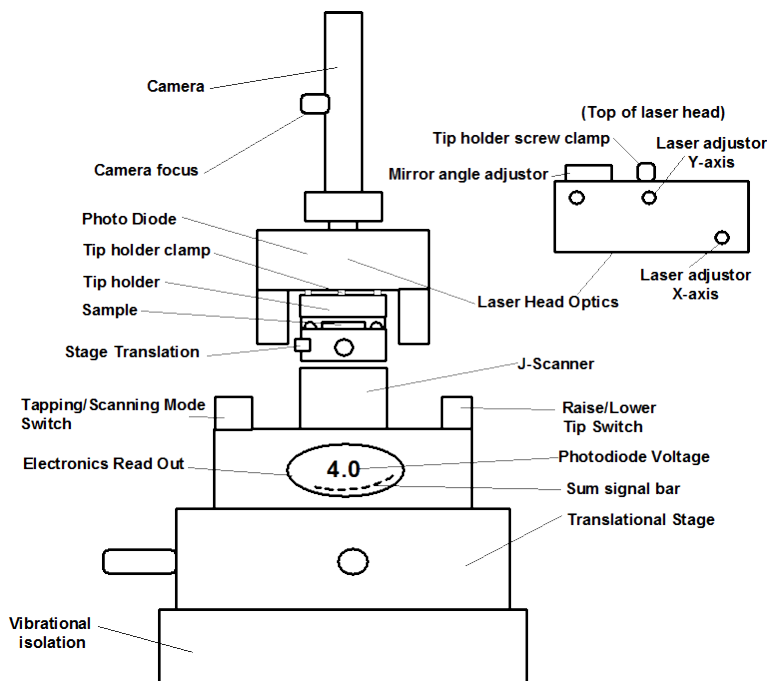


Figure 8.14: Schematic representation of the AFM.

8.2.2.2 Sample preparation

Most particulate samples are imaged by immobilizing them onto mica sheet, which is fixed to a metal puck (FIGURE 1). Samples that are in a solvent are easily deposited. To make a sample holder a sheet of Mica is punched out and stuck to double-sided carbon tape on a metal puck. In order to ensure a pristine surface, the mica sheet is cleaved by removing the top sheet with Scotch™ tape to reveal a pristine layer underneath. The sample can be spin coated onto the mica or air dried.

The spin coat method;

- Use double-sided carbon sticky tape to secure the puck on the spin coater.
- Load the sample by drop casting the sample solution onto the mica surface.
- The sample must be dry to ensure that the tip remains clean.

8.2.2.3 Puck and tip mounting

8.2.2.3.1 Puck mounting

Step 1. Place the sample puck in the magnetic sample holder, and center the sample.

Step 2. Verify that the AFM head is sufficiently raised to clear the sample with the probe. The sample plane is lower than the plane defined by the three balls. The sample should sit below the nubs. Use the lever on the right side of the J-scanner to adjust the height. (N.B. the labels up and down refer to the tip. “Tip up” moves the sample holder down to safety, and tip down moves the sample up. Use caution when moving the sample up.)

- Step 3. Select the appropriate cantilever for the desired imaging mode. The tips are fragile and expensive (ca. \$20 per tip) so handle with care.
- Contact AFM use a silicon nitride tip (NP).
 - Tapping AFM use a silicon tip (TESP).

8.2.2.3.2 Tip mounting and alignment

- Step 1. Mount a tip using the appropriate fine tweezers. Use the tweezers carefully to avoid possible misalignment. Work on a white surface (a piece of paper or a paper towel) so that the cantilever can be easily seen. The delicate part of the tip the cantilever is located at the beveled end and should not be handled at that end (shown in Figure 8.15). The tips are stored on a tacky gel tape. Use care, as dropping the tip will break the cantilever. Think carefully about how you approach the tip with the tweezers. Generally gripping it from the side is the best option. Once the tip is being held by the tweezers it needs to be placed in the tip holder clamp. With one hand holding the tweezers, use the other hand to open the clip by pressing down on the whole holder while it is lying on a flat hard surface. Once the clip is raised by downward pressure insert the tip (Figure 8.16a). Make sure the tip is seated firmly and that the back end is in contact with the end of the probe groove, there is a circular hole in the clamp. When the clamp holds the tip the hole should look like a half moon, with half filled with the back straight end of the tip. The groove is larger than the tip, so try to put the tip in the same place each time you replace it to improve reproducibility.
- Step 2. Carefully place the tip holder onto the three nubs to gently hold it in place. Bring the holder in at angle to avoid scraping it against the sample (Figure 8.16b).
- Step 3. Tighten the clamping screw located on the back of the AFM head to secure the cantilever holder and to guarantee electrical contact. The screw is on the back of the laser head, at the center.
- Step 4. Find the cantilever on the video display. Move the translational stage to find it.
- Step 5. Adjust the focusing knob of the optical microscope (located above AFM head) to focus on the cantilever tip. Tightening the focus knob moves the camera up. Focus on the dark blob on the right hand side of the screen as that is the cantilever.
- Step 6. Focus on the top mica surface, being careful not to focus on the bottom surface between the top of the double-sided carbon tape and the mica surface. Generally you will see a bubble trapped between the carbon tape and the mica surface. If you are focused on the top surface you can frequently see the reflection of the tip on the mica surface. The real focus is half way between the two cantilever focus points.
- Step 7. Slowly lower the tip down to the surface, if the camera is focused properly onto the surface the cantilever tip will gradually come into view. Keep lowering until the two tips images converge into one. Please note that you can crash the tip into the surface if you go past this point. This is damaging to the tip and may not be possible to obtain an image if it happens, and the tip may have to be replaced. You will know if this happens when looking at the cantilever tip if it goes from black to bright white. At this point the tip is in contact with the surface and turns white as it is not reflecting light back into the photo-diode, but instead into the camera.
- Step 8. Find the laser spot, if the spot is not visible on the camera screen look at the cantilever holder and see if it was visible. It helps to lower the brightness of the white light, use the translational stage again to search for it.
- Step 9. Once the laser spot has been located use the X and Y laser adjustment knobs to align the laser spot roughly onto the tip of the cantilever.
- Step 10. Maximize the sum signal using the photo-detector mirror lever located on the back of the head and the laser X and Y translation. The maximized sum value should be approximately 4 V.
- Step 11. To ensure that the laser is centered on the photodiode, zero the detector signals using the mirror adjustment knobs located on the top and back of the head. The knob on the top of the head adjusts vertical deflection, and the knob at the rear of the head adjusts horizontal deflection. The range is -9.9 V and 9.9 V. The number will change slowly at the extremes of the range and quickly around 0 V.

Ideally, the zeroed signal should be between ± 0.1 V. It will fluctuate during the experiment. If there is steady drift, you can adjust it during the experiment. If the number won't settle down, the laser could be at a bad position on the cantilever. Move the laser spot and repeat (Figure 8.17).

Step 12. Focus again on the sample surface.

Step 13. The sample surface can still be moved with respect to the camera via the sample stage. In choosing a place to image nanoparticles, avoid anything that you can see on the sample surface. The scale on the screen is $18 \mu\text{m}$ per cm.

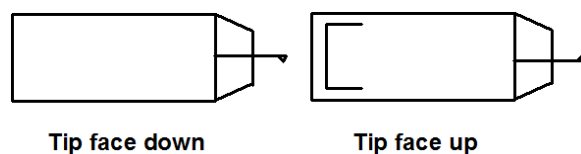


Figure 8.15: Schematic views of the AFM tip.

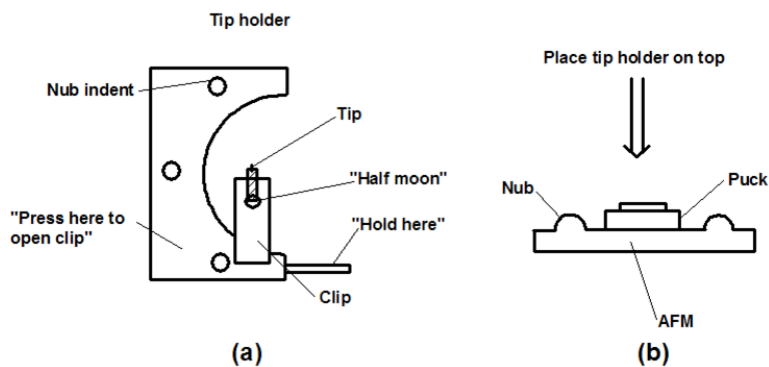


Figure 8.16: Schematic view of (a) the tip holder and (b) the tip holder location in the AFM.

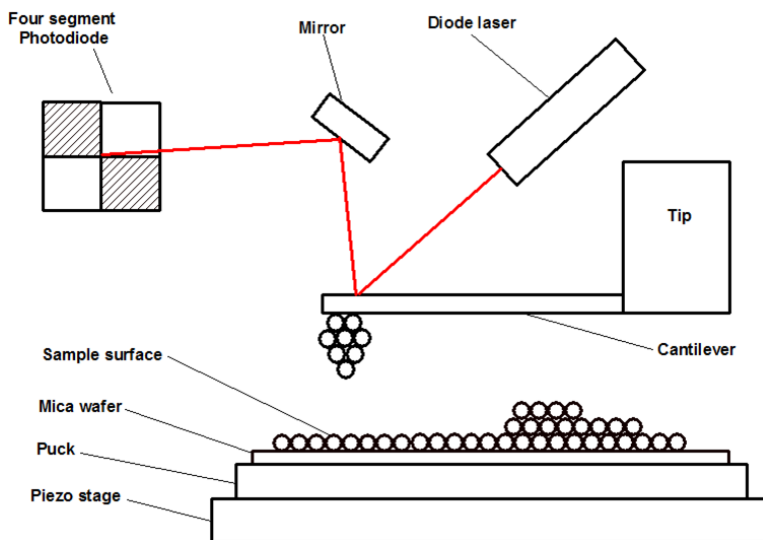


Figure 8.17: Schematic of the laser set-up.

8.2.2.4 Tip tuning

- Step 1. Log onto computer.
- Step 2. The software is called Nanoscope. Close the version dialog box. Typically the screen on the left will allow adjustment of software parameters, and the screen on the right will show the data.
- Step 3. On the adjustment screen, the two icons are to adjust the microscope (a picture of a microscope) and to perform data analysis (a picture of a rainbow). Click the microscope icon.
- Step 4. Under the microscope pull down menu, choose profile and select tapping AFM. Don't use another users profile. Use the "tapping" AFM.
- Step 5. Before beginning tapping mode, the cantilever must be tuned to ensure correct operation. Each tip has its own resonance frequency. The cantilever can be blindly auto-tuned or manually tuned. However the auto-tuning scheme can drive the amplitude so high as to damage the tip.

8.2.2.4.1 Auto-tuning

- Step 1. Click on the cantilever tune icon.
- Step 2. Click the auto-tune button. The computer will enter the tuning procedure, automatically entering such parameters as set point and drive amplitude. If tuned correctly, the drive frequency will be approximately 300 Hz.

8.2.2.4.2 Manually tuning

- Step 1. Click on the cantilever tune icon.
- Step 2. Select manual tuning under the sweep controls menu.

- Step 3. The plot is of amplitude (white) and phase (yellow) versus frequency. The sweep width is the X-range. The central frequency is the driving frequency which should be between 270-310 Hz. Typically the initial plot will not show any peaks, and the X and Y settings will need to be adjusted in order to see the resonance plot.
- Step 4. Widen the spectral window to about 100 Hz. The 270 – 310 Hz window where the driving frequency will be set needs to be visible.
- Step 5. To zoom in use the green line (this software is not click and drag!):
- Left click separation.
 - Left click position.
 - Right click to do something.
 - Right click to clear lines.
- Step 6. If a peak is clipped, change the drive amplitude. Ideally this will be between 15 and 20 mV, and should be below 500 mV. If a white line is not visible (there should be a white line along the bottom of the graph), the drive amplitude must be increased.
- Step 7. Ideally the peak will have a regular shape and only small shoulders. If there is a lot of noise, re-install the tip and things could improve. (Be careful as the auto-tuning scheme can drive the amplitude so high as to damage the tip.)
- Step 8. At this point, auto-tuning is okay. We can see that the parameters are reasonable. To continue the manual process, continue following these steps.
- Step 9. Adjust the drive amplitude so that the peak is at 2.0 V.
- Step 10. Amplitude set point while tuning corresponds to the vertical off set. If it is set to 0, the green line is 0.
- Step 11. Position the drive frequency not at the center of the peak, but instead at 5% toward the low energy (left) of the peak value. This offset is about $4/10^{\text{th}}$ of a division. Right click three times to execute this change. This accounts for the damping that occurs when the tip approaches the sample surface.
- Step 12. Left monitor - channel 2 dialogue box - click zero phase.

8.2.2.5 Image acquisition

- Step 1. Click the eyeball icon for image mode.
- Step 2. Parameter adjustments.
- Other controls.
 - Microscope mode: tapping.
 - Z-limit max height: 5.064 μm . This can be reduced if limited in Z-resolution.
 - Color table: 2.
 - Engage set point: 1.00.
 - Serial number of this scanner (double check since this has the factory parameter and is different from the other AFM).
 - Parameter update retract; disabled.
- Step 3. Scan controls:
- Scan size: 2 μm . Be careful when changing this value – it will automatically go between μm and nm (reasonable values are from 200 nm to 100 μm).
 - Aspect ratio: 1 to 1.
 - X and Y offset: 0.
 - Scan angle (like scan rotation): raster on the diagonal.
 - Scan rate: 1.97 Hz is fast, and 100 Hz is slow.
- Step 4. Feedback control:
- SPM: amplitude.
 - Integral gain: 0.5 (this parameter and the next parameter may be changed to improve image).
 - Proportional gain: 0.7.

- Amplitude set point: IV.
 - Drive frequency: from tuning.
 - Drive amplitude: from tuning.
- Step 5. Once all parameters are set, click engage (icon with green arrow down) to start engaging cantilever to sample surface and to begin image acquisition. The bottom of the screen should be “tip secured”. When the tip reaches the surface it automatically begins imaging.
- Step 6. If the amplitude set point is high, the cantilever moves far away from the surface, since the oscillation is damped as it approaches. While in free oscillation (set amplitude set point to 3), adjust drive amplitude so that the output voltage (seen on the scope) is 2 V. Big changes in this value while an experiment is running indicate that something is on the tip.
- Step 7. Select channel 2 data type – amplitude and height. Amplitude looks like a 3D image and is an excellent visualization tool or for a presentation. However the real data is the height data.
- Step 8. Bring the tip down (begin with amplitude set point to 2). The goal is to tap hard enough to get a good image, but not so hard as to damage the surface of the tip. Set to 3 clicks below just touching by further lowering amplitude set point with 3 left arrow clicks on the keyboard. The tip Z-center position scale on the right hand screen shows the extension on the piezo scanner. When the tip is properly adjusted, expect this value to be near the center.
- Step 9. Select view/scope mode (the scope icon). Check to see if trace and retrace are tracking each other. If so, the lines should look the same, but they probably will not overlap each other vertically or horizontally. If they are tracking well, then your tip is scanning the sample surface and you may return to view/image mode (the image icon). If they are not tracking well, adjust the scan rate, gains, and/or set point to improve the tracking. If tracing and retrace look completely different, you may need to decrease the set point to improve the tracking. If trace and retrace look completely different, you may need to decrease the set point one or two clicks with the left arrow key until they start having common features in both directions. Then reduce the scan rate: a reasonable value for scan sizes of 1-3 μm would be 2 Hz. Next try increasing the integral gain. As you increase the integral gain, the tracking should improve, although you will reach a value beyond which the noise will increase as the feedback loop starts to oscillate. If this happens, reduce gains, if trace and retrace still do not track satisfactorily, reduce the set point again. Once the tip is tracking the surface, choose view/image mode.
- Step 10. Integral gain controls the amount of integrated error signal used in the feedback calculation. The higher this parameter is set, the better the tip will track the same topography. However, if it is set too high, noise due to feedback oscillation will be introduced into the scan.
- Step 11. Proportional gain controls the amount of proportional error signal used in the feedback calculation.
- Step 12. Once amplitude set point is adjusted with the phase data, change channel 2 to amplitude. The data scale can be changed (it is the same as for display as it does not affect the data). In the amplitude image, lowering the voltage increases the contrast.
- Step 13. Move small amounts on the image surface with X and Y offset to avoid large, uninteresting objects. For example, setting the Y offset to -2 will remove features at the bottom of the image, thus shifting the image up. Changing it to -3 will then move the image one more unit up. Make sure you are using μm and not nm if you expect to see a real change.
- Step 14. To move further, disengage the tip (click the red up arrow icon so that the tip moves up 25 μm and secures). Move upper translational stage to keep the tip in view in the light camera. Re-engage the tip.
- Step 15. If the shadow in the image is drawn out, the amplitude set point should be lowered even further. The area on the image that is being drawn is controlled by the frame pull-down menu (and the up and down arrows). Lower the set point and redraw the same neighborhood to see if there is improvement. The proportional and integral gain can also be adjusted.
- Step 16. The frame window allows you to restart from the top, bottom, or a particular line.
- Step 17. Another way to adjust the amplitude set point value is to click on signal scope to ensure trace and retrace overlap. To stop Y rastering, slow scan axis.
- Step 18. To take a better image, increase the number of lines (512 is max), decrease the speed (1 Hz), and lower

the amplitude set point. The resolution is about 10 nm in the X and Y directions due to the size of the tip. The resolution in the Z direction is less than 1 nm.

- Step 19. Changing the scan size allows us to zoom in on features. You can zoom in on a center point by using zoom in box (left clicking to toggle between box position and size), or you can manually enter a scan size on the left hand screen.
- Step 20. Click on capture (the camera icon) to grab images. To speed things up, restart the scan at an edge to grab a new image after making any changes in the scan and feedback parameters. When parameters are changed, the capture option will toggle to “next”. There is a forced capture option, which allows you to collect an image even if parameters have been switched during the capture. It is not completely reliable.
- Step 21. To change the file name, select capture filename under the capture menu. The file will be saved in the!directory which is *d:\capture*. To save the picture, under the utility pull-down menu select TIFF export. The zip drive is *G:*.

8.2.2.6 Image analysis

- Step 1. Analysis involves flattening the image and measuring various particle dimensions, click the spectrum button.
- Step 2. Select the height data (image pull-down menu, select left or right image). The new icons in the “analysis” menu are:
- Thumbnails.
 - Top view.
 - Side view.
 - Section analysis.
 - Roughness.
 - Rolling pin (flattening).
 - Plane auto-fit.
- Step 3. To remove the bands (striping) in the image, select the rolling pin. The order of flattening is the order of the baseline correction. A raw offset is 0 order, a straight sloping line is order 1. Typically a second order correction is chosen to remove “scanner bow” which are the dark troughs on the image plane.
- Step 4. To remove more shadows, draw exclusion boxes over large objects and then re-flatten. Be sure to save the file under a new name. The default is to overwrite it.
- Step 5. In section analysis, use the multiple cursor option to measure a particle in all dimensions. Select fixed cursor. You can save pictures of this information, but things must be written down! There is also a particle analysis menu.
- Step 6. Disengage the cantilever and make sure that the cantilever is in secure mode before you move the cantilever to the other spots or change to another sample.
- Step 7. Loosen the clamp to remove the tip and holder.
- Step 8. Remove the tip and replace it onto the gel sticky tape using the fine tweezers.
- Step 9. Recover the sample with tweezers.
- Step 10. Close the program.
- Step 11. Log out of the instrument.
- Step 12. After the experiment, turn off the monitor and the power of the light source. Leave the controller on.
- Step 13. Sign out in the log book.

8.2.2.7 Bibliography

- R. Thaner and A. R. Barron, *Atomic Force Microscopy*, Connexions Web site. <http://cnx.org/content/m34664/1.1/> (Section 8.2.1), Jun 29, 2010.

- L. Zeng and A. R. Barron, *Characterization of Covalently Functionalized Single-Walled Carbon Nanotubes*, Connexions Web site. <http://cnx.org/content/m22299/1.4/> (Section 7.7), Jan 7, 2010.

8.3 SEM and its Applications for Polymer Science⁵

8.3.1 Introduction

The scanning electron microscope (SEM) is a very useful imaging technique that utilized a beam of electrons to acquire high magnification images of specimens. Very similar to the transmission electron microscope (TEM), the SEM maps the reflected electrons and allows imaging of thick (\sim mm) samples, whereas the TEM requires extremely thin specimens for imaging; however, the SEM has lower magnifications. Although both SEM and TEM use an electron beam, the image is formed very differently and users should be aware of when each microscope is advantageous.

8.3.2 Microscopy physics

8.3.2.1 Image formation

All microscopes serve to enlarge the size of an object and allow people to view smaller regions within the sample. Microscopes form optical images and although instruments like the SEM have extremely high magnifications, the physics of the image formation are very basic. The simplest magnification lens can be seen in Figure 8.18. The formula for magnification is shown in (8.20), where M is magnification, f is focal length, u is the distance between object and lens, and v is distance from lens to the image.

$$M = \frac{f}{u - f} = \frac{v - f}{f} \quad (8.20)$$

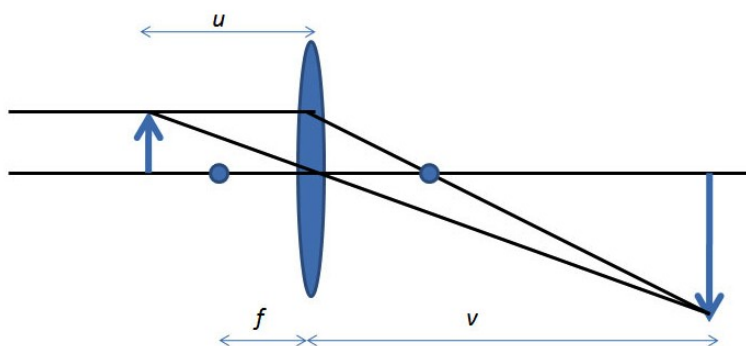


Figure 8.18: Basic microscope diagram illustrating inverted image and distances u , f and v .

Multistage microscopes can amplify the magnification of the original object even more as shown in Figure 8.19. Where magnification is now calculated from (8.21), where f_1 , f_2 are focal distances with

⁵This content is available online at <http://cnx.org/content/m38344/1.1/>.

respect to the first and second lens and v_1 , v_2 are the distances from the lens to the magnified image of first and second lens, respectively.

$$M = \frac{(v_1 - f_1)(v_2 - f_2)}{f_1 f_2} \quad (8.21)$$

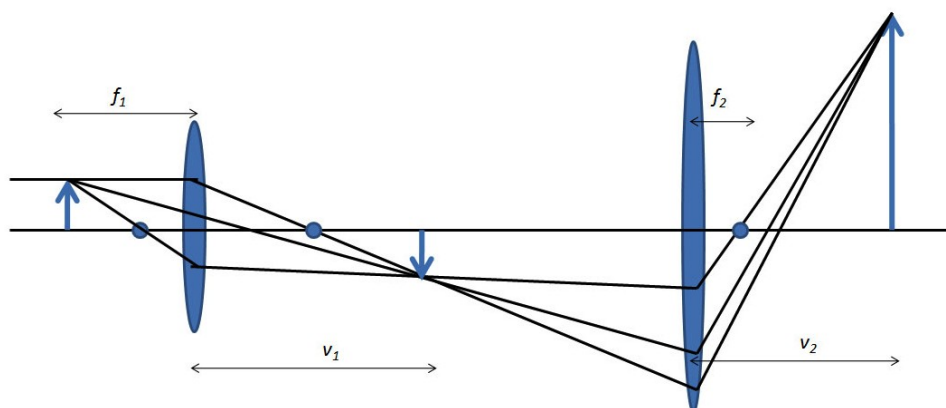


Figure 8.19: A schematic diagram of the optics used in a multistage microscope.

In reality, the objects we wish to magnify need to be illuminated. Whether or not the sample is thin enough to transmit light divides the microscope into two arenas. SEM is used for samples that do not transmit light, whereas the TEM (transmission electron microscope) requires transparent samples. Due to the many frequencies of light from the introduced source, a condenser system is added to control the brightness and narrow the range of viewing to reduce aberrations, which distort the magnified image.

8.3.3 Electron microscopes

Microscope images can be formed instantaneous (as in the optical microscope or TEM) or by rastering (scanning) a beam across the sample and forming the image point-by-point. The latter is how SEM images are formed. It is important to understand the basic principles behind SEM that define properties and limitations of the image.

8.3.3.1 Resolution

The resolution of a microscope is defined as the smallest distance between two features that can be uniquely identified (also called resolving power). There are many limits to the maximum resolution of the SEM and other microscopes, such as imperfect lenses and diffraction effects. Each single beam of light, once passed through a lens, forms a series of cones called an *airy ring* (see Figure 8.20). For a given wavelength of light, the central spot size is inversely proportional to the aperture size (i.e., large aperture yields small spot size) and high resolution demands a small spot size.

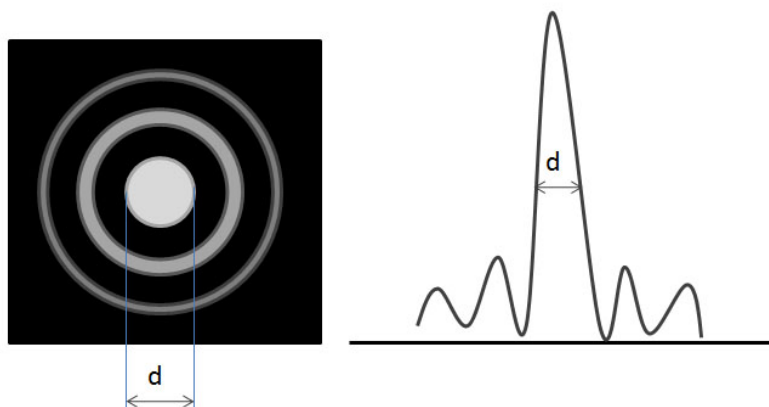


Figure 8.20: Airy ring illustrating center intensity (left) and intensity as a function of distance (right).

Aberrations distort the image and we try to minimize the effect as much as possible. Chromatic aberrations are caused by the multiple wavelengths present in *white* light. Spherical aberrations are formed by focusing inside and outside the ideal focal length and caused by the imperfections within the objective lenses. Astigmatism is because of further distortions in the lens. All aberrations decrease the overall resolution of the microscope.

8.3.3.2 Electrons

Electrons are charged particles and can interact with air molecules therefore the SEM and TEM instruments require extremely high vacuum to obtain images (10^{-7} atm). High vacuum ensures that very few air molecules are in the electron beam column. If the electron beam interacts with an air molecule, the air will become ionized and damage the beam filament, which is very costly to repair. The charge of the electron allows scanning and also inherently has a very small deflection angle off the source of the beam.

The electrons are generated with a thermionic filament. A tungsten (W) or LaB_6 filament is chosen based on the needs of the user. LaB_6 is much more expensive and tungsten filaments meet the needs of the average user. The microscope can be operated as field emission (tungsten filament).

8.3.3.3 Electron scattering

To accurately interpret electron microscopy images, the user must be familiar with how high energy electrons can interact with the sample and how these interactions affect the image. The probability that a particular electron will be scattered in a certain way is either described by the cross section, σ , or mean free path, λ , which is the average distance which an electron travels before being scattered.

8.3.3.3.1 Elastic scatter

Elastic scatter, or Rutherford scattering, is defined as a process which deflects an electron but does not decrease its energy. The wavelength of the scattered electron can be detected and is proportional to the atomic number. Elastically scattered electrons have significantly more energy than other types and provide mass contrast imaging. The mean free path, λ , is larger for smaller atoms meaning that the electron travels farther.

8.3.3.3.2 Inelastic scatter

Any process that causes the incoming electron to lose a detectable amount of energy is considered inelastic scattering. The two most common types of inelastic scatter are phonon scattering and plasmon scattering. Phonon scattering occurs when a primary electron loses energy by exciting a phonon, atomic vibrations in a solid, and heats the sample a small amount. A Plasmon is an oscillation within the bulk electrons in the conduction band for metals. Plasmon scattering occurs when an electron interacts with the sample and produces plasmons, which typically have 5 - 30 eV energy loss and small λ .

8.3.3.3.3 Secondary effects

A secondary effect is a term describing any event which may be detected *outside* the specimen and is essentially how images are formed. To form an image, the electron must interact with the sample in one of the aforementioned ways and *escape* from the sample and be detected. *Secondary electrons (SE)* are the most common electrons used for imaging due to high abundance and are defined, rather arbitrarily, as electrons with less than 50 eV energy after exiting the sample. *Backscattered electrons (BSE)* leave the sample quickly and retain a high amount of energy; however there is a much lower yield of BSE. Backscattered electrons are used in many different imaging modes. Refer to Figure 8.21 for a diagram of interaction depths corresponding to various electron interactions.

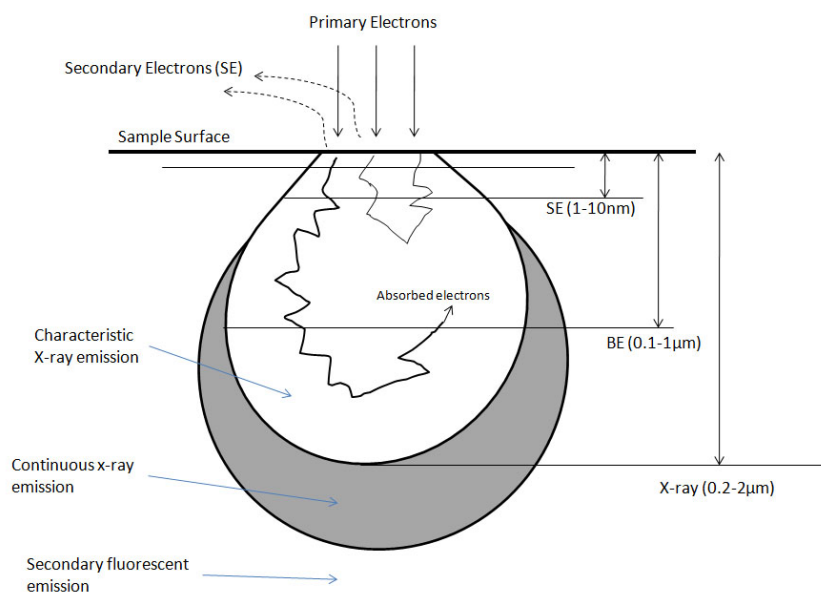


Figure 8.21: Diagram illustrating the depths at which various sample interactions occur.

8.3.4 SEM Construction

The SEM is made of several main components: electron gun, condenser lens, scan coils, detectors, specimen, and lenses (see Figure 8.22). Today, portable SEMs are available but the typical size is about 6 feet tall and contains the microscope column and the control console.

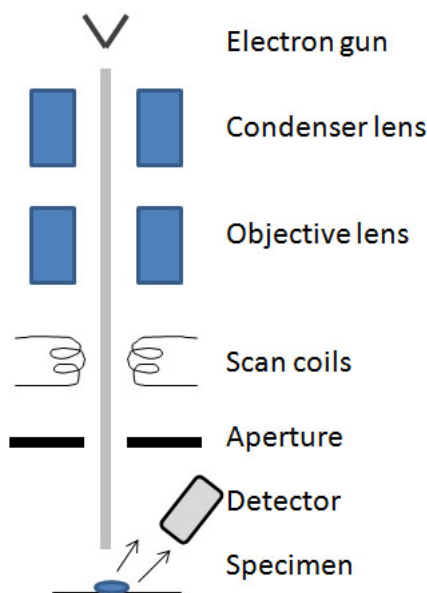


Figure 8.22: Schematic drawing of the SEM illustrating placement of electron generation, collimation process, sample interaction and electron detection.

A special feature of the SEM and TEM is known as *depth of focus*, dv/du the range of positions (depths) at which the image can be viewed with good focus, see (8.22). This allows the user to see more than a singular plane of a specified height in focus and essentially allows a range of three dimensional imaging.

$$\frac{dv}{du} = \frac{-v^2}{u^2} = -M^2 \quad (8.22)$$

8.3.4.1 Electron detectors (image formation)

The secondary electron detector (SED) is the main source of SEM images since a large majority of the electrons emitted from the sample are less than 50 eV. These electrons form textural images but cannot determine composition. The SEM may also be equipped with a backscatter electron detector (BSED) which collects the higher energy BSE's. Backscattered electrons are very sensitive to atomic number and can determine qualitative information about nuclei present (i.e., how much Fe is in the sample). Topographic images are taken by tilting the specimen 20 - 40° toward the detector. With the sample tilted, electrons are more likely to scatter off the top of the sample rather than interact within it, thus yielding information about the surface.

8.3.5 Sample preparation

The most effective SEM sample will be at least as thick as the interaction volume; depending on the image technique you are using (typically at least 2 μm). For the best contrast, the sample must be conductive or the sample can be sputter-coated with a metal (such as Au, Pt, W, and Ti). Metals and other materials that are naturally conductive do not need to be coated and need very little sample preparation.

8.3.6 SEM of polymers

As previously discussed, to view features that are smaller than the wavelength of light, an electron microscope must be used. The electron beam requires extremely high vacuum to protect the filament and electrons must be able to adequately interact with the sample. Polymers are typically long chains of repeating units composed primarily of “lighter” (low atomic number) elements such as carbon, hydrogen, nitrogen, and oxygen. These lighter elements have fewer interactions with the electron beam which yields poor contrast, so often times a stain or coating is required to view polymer samples. SEM imaging requires a conductive surface, so a large majority of polymer samples are sputter coated with metals, such as gold.

The decision to view a polymer sample with an SEM (versus a TEM for example) should be evaluated based on the feature size you expect the sample to have. Generally, if you expect the polymer sample to have features, or even individual molecules, over 100 nm in size you can safely choose SEM to view your sample. For much smaller features, the TEM may yield better results, but requires much different sample preparation than will be described here.

8.3.6.1 Polymer sample preparation techniques

8.3.6.1.1 Sputter coating

A sputter coater may be purchased that deposits single layers of gold, gold-palladium, tungsten, chromium, platinum, titanium, or other metals in a very controlled thickness pattern. It is possible, and desirable, to coat only a few nm's of metal onto the sample surface.

8.3.6.1.2 Spin coating

Many polymer films are depositing via a spin coater which spins a substrate (often ITO glass) and drops of polymer liquid are dispersed an even thickness on top of the substrate.

8.3.6.1.3 Staining

Another option for polymer sample preparation is staining the sample. Stains act in different ways, but typical stains for polymers are osmium tetroxide (OsO_4), ruthenium tetroxide (RuO_4) phosphotungstic acid ($\text{H}_3\text{PW}_{12}\text{O}_{40}$), hydrazine (N_2H_4), and silver sulfide (Ag_2S).

8.3.7 Examples

8.3.7.1 Comb-block copolymer (microstructure of cast film)

- Cast polymer film (see Figure 8.23).
- To view interior structure, the film was cut with a microtome or razor blade after the film was frozen in liquid N_2 and fractured.
- Stained with RuO_4 vapor (after cutting).
- Structure measurements were averaged over a minimum of 25 measurements.

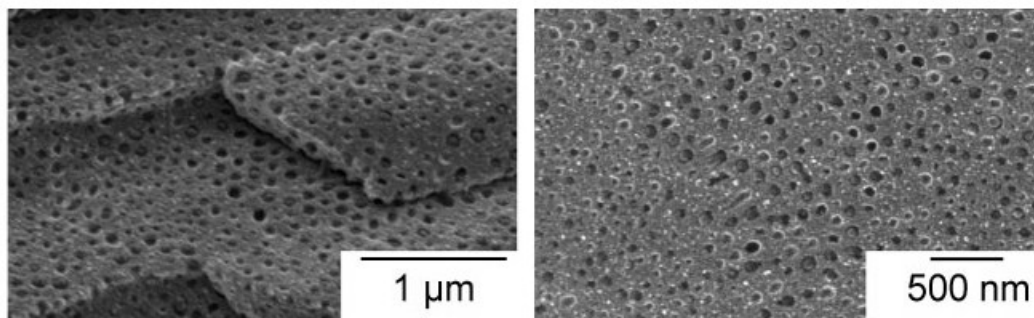


Figure 8.23: SEM micrograph of comb block copolymer showing spherical morphology and long range order. Adapted from M. B. Runge and N. B. Bowden, *J. Am. Chem. Soc.*, 2007, **129**, 10551. Copyright: American Chemical Society (2007).

8.3.7.1.1 Polystyrene-poly lactide bottlebrush copolymers (lamellar spacing)

- Pressed polymer samples into disks and annealed for 16 h at 170 °C.
- To determine ordered morphologies, the disk was fractured (see Figure 8.24).
- Used SEM to verify lamellar spacing from USAXS.

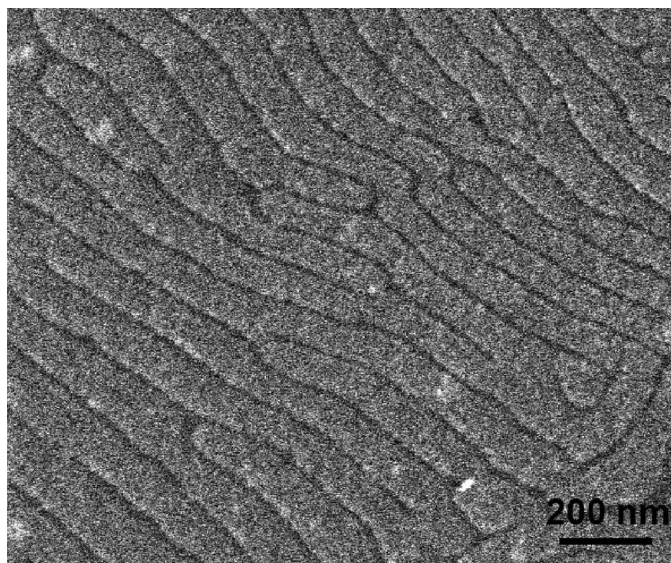


Figure 8.24: SEM image of a fractured piece of polymer SL-1. Adapted from J. Rzyev, *Macromolecules*, 2009, **42**, 2135. Copyright: American Chemical Society (2009).

8.3.7.1.2 SWNTs in ultrahigh molecular weight polyethylene

- Dispersed SWNTs in interactive polymer.
- Samples were sputter-coated in gold to enhance contrast.
- The films were solution-crystallized and the cross-section was imaged.
- Environmental SEM (ESEM) was used to show morphologies of composite materials.
- $WD = 7 \text{ mm}$.
- Study was conducted to image sample before and after drawing of film.
- Images confirmed the uniform distribution of SWNT in PE (Figure 8.25).
- $M_W = 10,000 \text{ Dalton}$.
- Study performed to compare transparency before and after UV irradiation.

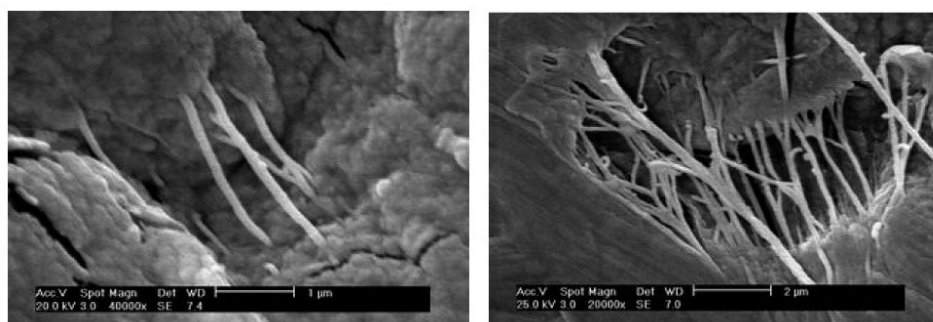


Figure 8.25: SEM images of crystallized SWNT-UHMWPE films before (left) and after (right) drawing at $120 \text{ }^\circ\text{C}$. Adapted from Q. Zhang, D. R. Lippits, and S. Rastogi, *Macromolecules*, 2006, **39**, 658. Copyright: American Chemical Society (2006).

8.3.7.1.3 Nanostructures in conjugated polymers (nanoporous films)

- Polymer and NP were processed into thin films and heated to crosslink.
- SEM was used to characterize morphology and crystalline structure (Figure 8.26).
- SEM was used to determine porosity and pore size.
- Magnified orders of $200 \text{ nm} - 1 \text{ } \mu\text{m}$.
- $WD = 8 \text{ mm}$.
- $M_W = 23,000 \text{ Daltons}$
- Sample prep: spin coating a solution of poly-(thiophene ester) with copper NPs suspended on to ITO coated glass slides. Ziess, Supra 35

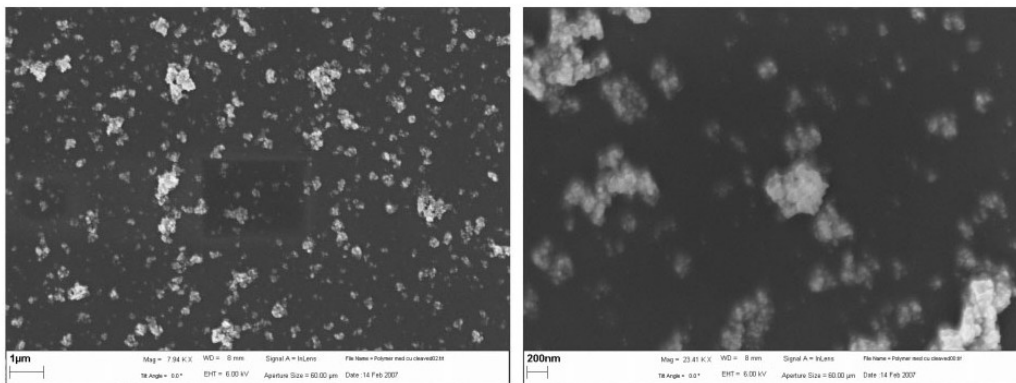


Figure 8.26: SEM images of thermocleaved film loaded with nanoparticles with scale bar 1 μm . Adapted from J. W. Andreasen, M. Jorgensen, and F. C. Krebs, *Macromolecules*, 2007, **40**, 7758. Copyright: American Chemical Society (2007).

8.3.7.1.4 Cryo-SEM colloid polystyrene latex particles (fracture patterns)

- Used cryogenic SEM (cryo-SEM) to visualize the microstructure of particles (Figure 8.27).
- Particles were immobilized by fast-freezing in liquid N_2 at $-196\text{ }^\circ\text{C}$.
- Sample is fractured ($-196\text{ }^\circ\text{C}$) to expose cross section.
- 3 nm sputter coated with platinum.
- Shapes of the nanoparticles after fracture were evaluated as a function of crosslink density.

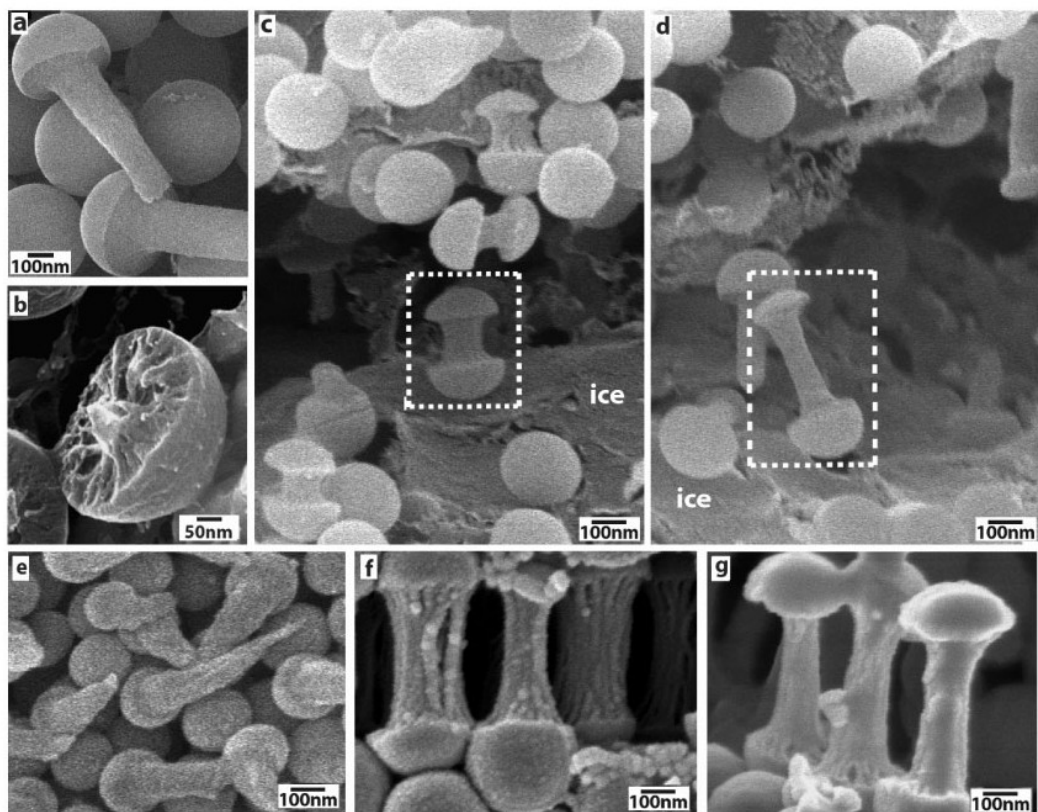


Figure 8.27: Cryo-SEM images of plastically drawn polystyrene and latex particles. Adapted from H. Ge, C. L. Zhao, S. Porzio, L. Zhuo, H. T. Davis, and L. E. Scriven, *Macromolecules*, 2006, **39**, 5531. Copyright: American Chemical Society (2006).

8.3.8 Bibliography

- H. Ge, C. L. Zhao, S. Porzio, L. Zhuo, H. T. Davis, and L. E. Scriven, *Macromolecules*, 2006, **39**, 5531.
- J. Rzayev, *Macromolecules*, 2009, **42**, 2135.
- J. W. Andreasen, M. Jorgensen, and F. C. Krebs, *Macromolecules*, 2007, **40**, 7758.
- M. B. Runge and N. B. Bowden, *J. Am. Chem. Soc.*, 2007, **129**, 10551.
- P. J. Goodhew, J. Humphreys, and R. Beanland, *Electron Microscopy and Analysis*, Taylor & Francis Inc., New York (2001).
- Q. Zhang, D. R. Lippits, and S. Rastogi, *Macromolecules*, 2006, **39**, 658.

8.4 Catalyst Characterization Using Thermal Conductivity Detector⁶

8.4.1 Introduction

A catalyst is a "substance that accelerates the rate of chemical reactions without being consumed". Some reactions, such as the hydrodechlorination of TCE, (8.23), don't occur spontaneously, but can occur in the presence of a catalyst.



Metal dispersion is a common term within the catalyst industry. The term refers to the amount of metal that is active for a specific reaction. Let's assume a catalyst material has a composition of 1 wt% palladium and 99% alumina (Al_2O_3) (Figure 8.28). Even though the catalyst material has 1 wt% of palladium, not all the palladium is active. The material might be oxidized due to air exposure or some of the material is not exposed to the surface (Figure 8.29), hence it can't participate in the reaction. For this reason it is important to characterize the material.



Figure 8.28: A photograph of a sample of commercially available 1 wt% Pd/ Al_2O_3 .

⁶This content is available online at <<http://cnx.org/content/m43579/1.1/>>.



Figure 8.29: Representation of Pd nanoparticles on Al_2O_3 . Some palladium atoms are exposed to the surface, while some other lay below the surface atoms and are not accessible for reaction.

In order for Pd to react according to (8.23), it needs to be in the metallic form. Any oxidized palladium will be inactive. Thus, it is important to determine the oxidation state of the Pd atoms on the surface of the material. This can be accomplished using an experiment called temperature programmed reduction (TPR). Subsequently, the percentage of active palladium can be determined by hydrogen chemisorption. The percentage of active metal is an important parameter when comparing the performance of multiple catalyst. Usually the rate of reaction is normalized by the amount of active catalyst.

8.4.2 Principles of thermal conductivity

Thermal conductivity is the ability of a chemical specie to conduct heat. Each gas has a different thermal conductivity. The units of thermal conductivity in the international system of units are $\text{W}/\text{m}\cdot\text{K}$. Table 8.2, shows the thermal conductivity of some common gasses.

Gas	Thermal conductivity ($\text{W}/\text{m}\cdot\text{K}$)
Hydrogen	0.18050
Argon	0.01772
Helium	0.15130
Carbon Monoxide	0.02614

Table 8.2: Thermal conductivity values for common gasses.

8.4.3 Thermal conductivity detector

A thermal conductivity detector has four filaments that change resistance according to the thermal conductivity of the gas flowing over it. Two filaments measure the reference gas and the other two measures the sample gas. The detector is isothermal; it will increase or decrease the voltage in each of the resistors in order to maintain a constant temperature. The temperature of the detector is $125\text{ }^\circ\text{C}$. When both the reference and samples gas have the same composition and same flow rate, the resistors are balanced and the detector will zero the signal. If there is a change in flow rate or in the gas composition the detector will react

to maintain the constant temperature. The detector circuitry can be described using a Wheatstone bridge configuration as shown in Figure 8.30. If the gas flowing through the sample has a higher thermal conductivity the filament will cool down, the detector will apply a higher voltage to keep a constant temperature and this will be recorded as a positive signal.

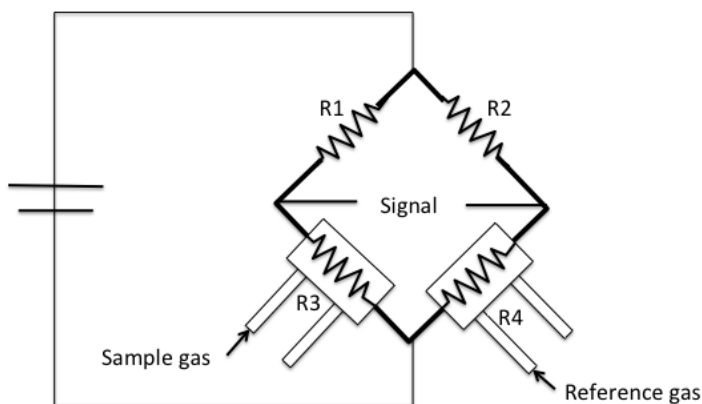


Figure 8.30: A simplified circuit diagram of a thermal conductivity detector.

This detector is part of a typical commercial instrument such as a Micromeritics AutoChem 2920 (Figure 8.31). This instrument is an automated analyzer with the ability to perform chemical adsorption and temperature-programmed reactions on a catalyst, catalyst support, or other materials.



Figure 8.31: A photograph of a Micromeritics AutoChem 2920.

8.4.4 Temperature programmed reduction (TPR)

TPR will determine the number of reducible species on a catalyst and will tell at what temperature each of these species was reduced. For example palladium is ordinarily found as Pd(0) or Pd(II), i.e., oxidation states 0 and +2. Pd(II) can be reduced at very low temperatures (5 - 10 °C) to Pd(0) following (8.24).



A 128.9 mg 1wt% Pd/Al₂O₃ samples is used for the experiment, Figure 8.32. Since we want to study the oxidation state of the commercial catalyst, no pre-treatment needs to be executed to the sample. A 10% hydrogen-argon mixture is used as analysis and reference gas. Argon has a low thermal conductivity and hydrogen has a much higher thermal conductivity. All gases will flow at 50 cm³/min. The TPR experiment will start at an initial temperature of 200 K, temperature ramp 10 K/min, and final temperature of 400 K. The H₂/Ar mixture is flowed through the sample, and past the detector in the analysis port. While in the reference port the mixture doesn't become in contact with the sample. When the analysis gas starts flowing over the sample, a baseline reading is established by the detector. The baseline is established at the initial temperature to ensure there is no reduction. While this gas is flowing, the temperature of the sample is increased linearly with time and the consumption of hydrogen is recorded. Hydrogen atoms react with oxygen atoms to form H₂O.

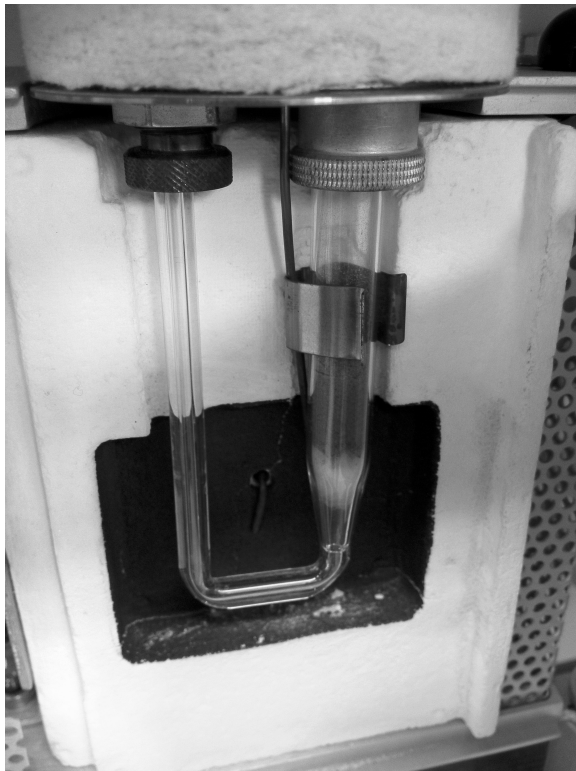


Figure 8.32: A sample of Pd/Al₂O₃ in a typical sample holder.

Water molecules are removed from the gas stream using a cold trap. As a result, the amount of hydrogen in the argon/hydrogen gas mixture decreases and the thermal conductivity of the mixture also decrease. The change is compared to the reference gas and yields to a hydrogen uptake volume. Figure 8.33 is a typical TPR profile for PdO.

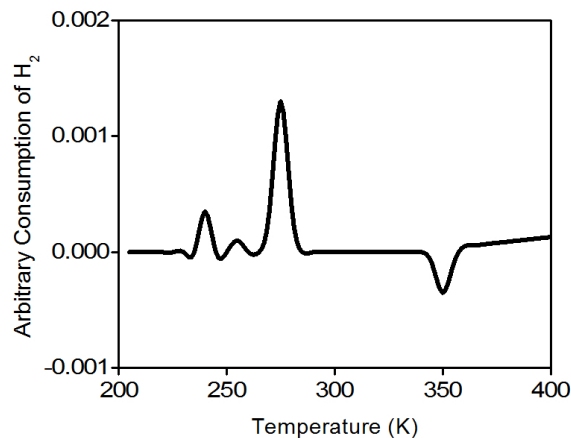


Figure 8.33: A typical TPR profile of PdO. Adapted from R. Zhang, J. A. Schwarz, A. Datye, and J. P. Baltrus, *J. Catal.*, 1992, **138**, 55.

8.4.5 Pulse chemisorption

Once the catalyst (1 wt% Pd/Al₂O₃) has been completely reduced, the user will be able to determine how much palladium is active. A pulse chemisorption experiment will determine active surface area, percentage of metal dispersion and particle size. Pulses of hydrogen will be introduced to the sample tube in order to interact with the sample. In each pulse hydrogen will undergo a dissociative adsorption on to palladium active sites until all palladium atoms have reacted. After all active sites have reacted, the hydrogen pulses emerge unchanged from the sample tube. The amount of hydrogen chemisorbed is calculated as the total amount of hydrogen injected minus the total amount eluted from the system.

8.4.6 Data collection for hydrogen pulse chemisorption

The sample from previous experiment (TPR) will be used for this experiment. Ultra high-purity argon will be used to purge the sample at a flow rate of 40 cm³/min. The sample will be heated to 200 °C in order to remove all chemisorbed hydrogen atoms from the Pd(0) surface. The sample is cooled down to 40 °C. Argon will be used as carrier gas at a flow of 40 cm³/min. Filaments temperature will be 175 °C and the detector temperature will be 110 °C. The injection loop has a volume of 0.03610 cm³ @ STP. As shown in Figure 8.34., hydrogen pulses will be injected in to the flow stream, carried by argon to become in contact and react with the sample. It should be noted that the first pulse of hydrogen was almost completely adsorbed by the sample. The second and third pulses show how the samples is been saturated. The positive value of the TCD detector is consistent with our assumptions. Since hydrogen has a higher thermal conductivity than argon, as it flows through the detector it will tend to cool down the filaments, the detector will then apply a positive voltage to the filaments in order to maintain a constant temperature.

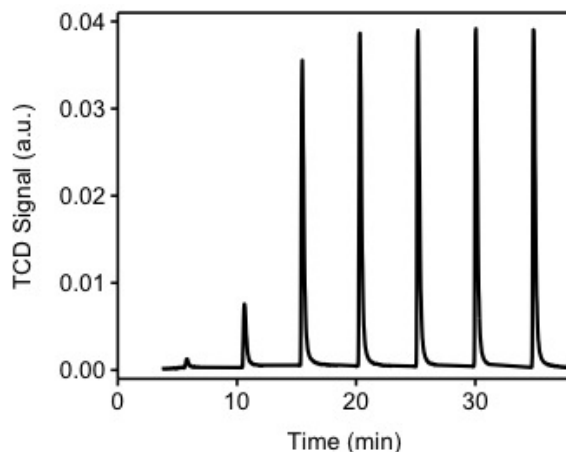


Figure 8.34: A typical hydrogen pulse chemisorption profile of 1 wt% Pd/Al₂O₃.

8.4.7 Pulse chemisorption data analysis

Table 8.3 shows the integration of the peaks from Figure 8.34. This integration is performed by an automated software provided with the instrument. It should be noted that the first pulse was completely consumed by the sample, the pulse was injected between time 0 and 5 minutes. From Figure 8.34 we observe that during the first four pulses, hydrogen is consumed by the sample. After the fourth pulse, it appears the sample is not consuming hydrogen. The experiment continues for a total of seven pulses, at this point the software determines that no consumption is occurring and stops the experiment. Pulse eight is denominated the "saturation peak", meaning the pulse at which no hydrogen was consumed.

Pulse n	Area
1	0
2	0.000471772
3	0.00247767
4	0.009846683
5	0.010348201
6	0.010030243
7	0.009967717
8	0.010580979

Table 8.3: Hydrogen pulse chemisorption data.

Using (8.25) the change in area (Δarea_n) is calculated for each peak pulse area (area_n) and compared to that of the saturation pulse area ($\text{area}_{\text{saturation}} = 0.010580979$). Each of these changes in area is proportional

to an amount of hydrogen consumed by the sample in each pulse. Table 8.4 Shows the calculated change in area.

$$\Delta\text{Area}_n = \text{Area}_{\text{saturation}} - \text{Area}_n \quad (8.25)$$

Pulse n	Area _n	ΔArea _n
1	0	0.010580979
2	0.000471772	0.0105338018
3	0.00247767	0.008103309
4	0.009846683	0.000734296
5	0.010348201	0.000232778
6	0.010030243	0.000550736
7	0.009967717	0.000613262
8	0.010580979	0

Table 8.4: Hydrogen pulse chemisorption data with ΔArea.

The Δarea_n values are then converted into hydrogen gas consumption using (8.26), where F_c is the area-to-volume conversion factor for hydrogen and SW is the weight of the sample. F_c is equal to 2.6465 cm³/peak area. Table 8.5 shows the results of the volume adsorbed and the cumulative volume adsorbed. Using the data on Table 8.5, a series of calculations can now be performed in order to have a better understanding of our catalyst properties.

$$V_{\text{adsorbed}} = \frac{\Delta\text{Area}_n \times F_c}{SW} \quad (8.26)$$

Pulse n	area _n	Δarea _n	V _{adsorbed} (cm ³ /g STP)	Cumulative quantity (cm ³ /g STP)
1	0	0.0105809790	0.2800256	0.2800256
2	0.000471772	0.0105338018	0.2787771	0.5588027
3	0.00247767	0.0081033090	0.2144541	0.7732567
4	0.009846683	0.0007342960	0.0194331	0.7926899
5	0.010348201	0.0002327780	0.0061605	0.7988504
6	0.010030243	0.0005507360	0.0145752	0.8134256

continued on next page

7	0.009967717	0.0006132620	0.0162300	0.8296556
8	0.010580979	0	0.0000000	0.8296556

Table 8.5: Includes the volume adsorbed per pulse and the cumulative volume adsorbed.

8.4.7.1 Gram molecular weight

Gram molecular weight is the weighted average of the number of moles of each active metal in the catalyst. Since this is a monometallic catalyst, the gram molecular weight is equal to the molecular weight of palladium (106.42 [g/mol]). The GMW_{Calc} is calculated using (8.27), where F is the fraction of sample weight for metal N and $W_{\text{atomic}N}$ is the gram molecular weight of metal N (g/g-mole). (8.28) shows the calculation for this experiment.

$$\text{GMW}_{\text{Calc}} = \frac{1}{\left(\frac{F_1}{W_{\text{atomic}1}}\right) + \left(\frac{F_2}{W_{\text{atomic}2}}\right) + \dots + \left(\frac{F_N}{W_{\text{atomic}N}}\right)} \quad (8.27)$$

$$\text{GMW}_{\text{Calc}} = \frac{1}{\left(\frac{F_1}{W_{\text{atomicPd}}}\right)} = \frac{W_{\text{atomicPd}}}{F_1} = \frac{106.42 \frac{\text{g}}{\text{g-mole}}}{1} = 106.42 \frac{\text{g}}{\text{g-mole}} \quad (8.28)$$

8.4.7.2 Metal dispersion

The metal dispersion is calculated using (8.29), where PD is the percent metal dispersion, V_s is the volume adsorbed (cm^3 at STP), SF_{Calc} is the calculated stoichiometry factor (equal to 2 for a palladium-hydrogen system), SW is the sample weight and GMW_{Calc} is the calculated gram molecular weight of the sample [g/g-mole]. Therefore, in (8.30) we obtain a metal dispersion of 6.03%.

$$PD = 100 \times \left(\frac{V_s \times \text{SF}_{\text{Calc}}}{SW \times 22414} \right) \times \text{GMW}_{\text{Calc}} \quad (8.29)$$

$$PD = 100 \times \left(\frac{0.8296556 [\text{cm}^3] \times 2}{0.1289 [\text{g}] \times 22414 \left[\frac{\text{cm}^3}{\text{mol}} \right]} \right) \times 106.42 \left[\frac{\text{g}}{\text{g-mol}} \right] = 6.03\% \quad (8.30)$$

8.4.7.3 Metallic surface area per gram of metal

The metallic surface area per gram of metal is calculated using (8.31), where $\text{SA}_{\text{Metallic}}$ is the metallic surface area (m^2/g of metal), SW_{Metal} is the active metal weight, SF_{Calc} is the calculated stoichiometric factor and SA_{Pd} is the cross sectional area of one palladium atom (nm^2). Thus, in (8.30) we obtain a metallic surface area of $2420.99 \text{ m}^2/\text{g-metal}$.

$$\text{SA}_{\text{Metallic}} = \left(\frac{V_s}{\text{SW}_{\text{Metal}} \times 22414} \right) \times (\text{SF}_{\text{Calc}}) \times (6.022 \times 10^{23}) \times \text{SA}_{\text{Pd}} \quad (8.31)$$

$$\text{SA}_{\text{Metallic}} = \left(\frac{0.8296556 [\text{cm}^3]}{0.01289 [\text{g}_{\text{metal}}] \times 22414 \left[\frac{\text{cm}^3}{\text{mol}} \right]} \right) \times (2) \times (6.022 \times 10^{23} \left[\frac{\text{atoms}}{\text{mol}} \right]) \times 0.07 \left[\frac{\text{nm}^2}{\text{atom}} \right] = 2420.99 \left[\frac{\text{m}^2}{\text{g-metal}} \right] \quad (8.32)$$

8.4.7.4 Active particle size

The active particle size is estimated using (8.33), where D_{Calc} is palladium metal density (g/cm^3), SW_{Metal} is the active metal weight, GMW_{Calc} is the calculated gram molecular weight ($\text{g}/\text{g-mole}$), and SA_{Pd} is the cross sectional area of one palladium atom (nm^2). As seen in (8.34) we obtain an optical particle size of 2.88 nm.

$$\text{APS} = \frac{6}{D_{\text{Calc}} \times \left(\frac{W_s}{GMW_{\text{Calc}}} \right) \times (6.022 \times 10^{23}) \times SA_{\text{Metallic}}} \quad (8.33)$$

$$\text{APS} = \frac{600}{(1.202 \times 10^{-20} \left[\frac{\text{g}_{\text{Pd}}}{\text{nm}^3} \right]) \times \left(\frac{0.001289[\text{g}]}{106.42 \left[\frac{\text{g}_{\text{Pd}}}{\text{mol}} \right]} \right) \times (6.022 \times 10^{23} \left[\frac{\text{atoms}}{\text{mol}} \right]) \times \left(2420.99 \left[\frac{\text{m}^2}{\text{g}_{\text{Pd}}} \right] \right)} = 2.88 \text{ nm} \quad (8.34)$$

In a commercial instrument, a summary report will be provided which summarizes the properties of our catalytic material. All the equations used during this example were extracted from the AutoChem 2920-User's Manual.

Properties	Value
Palladium atomic weight	106.4 g/mol
Atomic cross-sectional area	0.0787 nm ²
Metal density	12.02 g/cm ³
Palladium loading	1 wt%
Metal dispersion	6.03%
Metallic surface area	2420.99 m ² /g-metal
Active particle diameter (hemisphere)	2.88 nm

Table 8.6: Summary report provided by Micromeritics AuthoChem 2920.

8.4.8 References

- A. J. Canty, *Accounts Chem. Res.*, 1992, **25**, 83.
- H. S. Fogler, *Elements of Chemical Reaction Engineering*, Prentice-Hall, New York (1992).
- Micromeritics Instrument Corporation, *AutoChem 2920 – Automated catalyst characterization system – Operators Manual*, V4.01 (2009).
- M. O. Nutt, K. N. Heck, P. Alvarez, and M. S. Wong, *Appl. Catal. B-Environ.*, 2006, **69**, 115.
- M. O. Nutt, J. B. Hughes, and M. S. Wong, *Environ. Sci. Technol.*, 2005, **39**, 1346.
- P. A. Webb and C. Orr, *Analytical Methods in Fine Particle Technology*, Micromeritics Instrument Corp, 1997.
- R. Zhang, J. A. Schwarz, A. Datye, and J. P. Baltrus, *J. Catal.*, 1992, **138**, 55.

8.5 Nanoparticle Deposition Studies Using a Quartz Crystal Microbalance⁷

8.5.1 Overview

The working principle of a quartz crystal microbalance with dissipation (QCM-D) module is the utilization of the resonance properties of some piezoelectric of materials. A piezoelectric material is a material that exhibits an electrical field when a mechanical strain is applied. This phenomenon is also observed in the contrary where an applied electrical field produce a mechanical strain in the material. The material used is α -SiO₂ that produces a very stable and constant frequency. The direction and magnitude of the mechanical strain is directly dependent of the direction of the applied electrical field and the inherent physical properties of the crystal.

A special crystal cut is used, called AT-cut, which is obtain as wafers of the crystal of about 0.1 to 0.3 mm in width and 1 cm in diameter. The AT-cut is obtained when the wafer is cut at 35.25° of the main crystallographic axis of SiO₂. This special cut allows only one vibration mode, the shear mode, to be accessed and thus exploited for analytical purposes. When a electrical field is applied to the crystal wafer via metal electrodes, that are vapor-deposited in the surface, a mechanical shear is produced and maintained as long as the electrical field is applied. Since this electric field can be controlled by opening and closing an electrical circuit, a resonance within the crystal is formed (Figure 8.35).

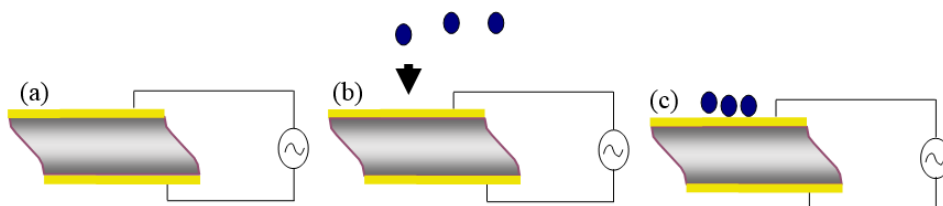


Figure 8.35: Schematic representation of the piezoelectric material: (a) a baseline is obtained by running the sensor without any flow or sample; (b) sample is starting to flow into the sensor; (c) sample deposited in the sensor change the frequency.

Since the frequency of the resonance is dependent of the characteristics of the crystal, an increase of mass, for example when the sample is loaded into the sensor would change the frequency change. This relation (8.35) was obtained by Sauerbrey in 1959, where Δm ($\text{ng}\cdot\text{cm}^{-2}$) is the areal mass, C ($17.7 \text{ ngcm}^{-2}\text{Hz}^{-1}$) is the vibrational constant (shear, effective area, etc.), n in Hz is the resonant overtone, and Δf is the change in frequency. The dependence of the change in the frequency can be related directly to the change in mass deposited in the sensor only when three conditions are met and assumed:

1. The mass deposited is small compared to the mass of the sensor.
2. It is rigid enough so that it vibrates with the sensor and does not suffer deformation.
3. The mass is evenly distributed among the surface of the sensor.

$$\Delta m = -C \frac{1}{n} \Delta f \quad (8.35)$$

⁷This content is available online at <<http://cnx.org/content/m46155/1.2/>>.

An important incorporation in recent equipment is the use of the dissipation factor. The inclusion of the dissipation factor takes into account the weakening of the frequency as it travels along the newly deposited mass. In a rigid layer the frequency is usually constant and travels through the newly formed mass without interruption, thus, the dissipation is not important. On the other hand, when the deposited material has a soft consistency the dissipation of the frequency is increased. This effect can be monitored and related directly to the nature of the mass deposited.

The applications of the QCM-D ranges from the deposition of nanoparticles into a surface, from the interaction of proteins within certain substrates. It can also monitor the bacterial amount of products when fed with different molecules, as the flexibility of the sensors into what can be deposited in them include nanoparticle, special functionalization or even cell and bacteria!

8.5.2 Experimental planning

In order to use QCM-D for studying the interaction of nanoparticles with a specific surface several steps must be followed. For demonstration purposes the following procedure will describe the use of a Q-Sense E4 with autosampler from Biolin Scientific. A summary is shown below as a quick guide to follow, but further details will be explained:

1. Surface election and cleaning according with the manufacturer recommendations.
2. Sample preparation including having the correct dilutions and enough sample for the running experiment.
3. Equipment cleaning and set up of the correct parameters for the experiment.
4. Data acquisition.
5. Data interpretation.

8.5.2.1 Surface election

The decision of what surface of the the sensor to use is the most important decision to make fore each study. Biolin has a large library of available coatings ranging from different compositions of pure elements and oxides (Figure 8.36) to specific binding proteins. It is important to take into account the different chemistries of the sensors and the results we are looking for. For example studying a protein with high sulfur content on a gold sensor can lead to a false deposition results, as gold and sulfur have a high affinity to form bonds. For the purpose of this example, a gold coated sensor will be used in the remainder of the discussion.



Figure 8.36: From left to right, silica (SiO_2), gold (Au), and iron oxide (Fe_2O_3) coated sensors. Each one is 1 cm in diameter.

8.5.2.2 Sensor cleaning

Since QCM-D relies on the amount of mass that is deposited into the surface of the sensor, a thorough cleaning is needed to ensure there is no contaminants on the surface that can lead to errors in the measurement. The procedure the manufacturer established to clean a gold sensor is as follows:

- Step 1. Put the sensor in the UV/ozone chamber for 10 minutes
- Step 2. Prepare 10 mL of a 5:1:1 solution of hydrogen peroxide:ammonia:water
- Step 3. Submerge in this solution at 75 °C for 5 minutes.
- Step 4. Rinse with copious amount of milliQ water.
- Step 5. Dry with inert gas.
- Step 6. Put the sensor in the UV/ozone chamber for 10 minutes as shown in Figure 8.37.

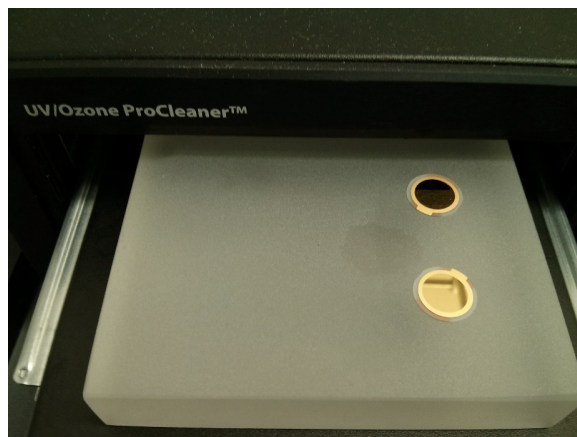


Figure 8.37: Gold sensors in loader of the UV/ozone chamber in the final step of the cleaning process.

Once the sensors are clean, extreme caution should be taken to avoid contamination of the surface. The sensors can be loaded in the flow chamber of the equipment making sure that the T-mark of the sensor matches the T mark of the chamber in order to make sure the electrodes are in constant contact. The correct position is shown in Figure 8.38.



Figure 8.38: Correct position of the sensor in the chamber.

8.5.2.3 Sample preparation

As the top range of mass that can be detected is merely micrograms, solutions must be prepared accordingly. For a typical run, a buffer solution is needed in which the deposition will be studied as well as, the sample

itself and a solution of 2% of sodium dodecylsulfate [$\text{CH}_3(\text{CH}_2)_{10}\text{CH}_2\text{OSO}_3\text{Na}$, SDS]. For this example we will be using nanoparticles of magnetic iron oxide (nMag) coated with PAMS, and as a buffer 8% NaCl in DI water.

- For the nanoparticles sample it is necessary to make sure the final concentration of the nanoparticles will not exceed 1 mM.
- For the buffer solution, it is enough to dissolve 8 g of NaCl in DI water.
- For the SDS solution, 2 g of SDS should be dissolved very slowly in approximate 200 mL of DI water, then 100 mL aliquots of DI water is added until the volume is 1 L. This is in order to avoid the formation of bubbles and foam in the solution.

8.5.2.4 Instrument preparation

Due to the sensitivity of the equipment, it is important to rinse and clean the tubing before loading any sample or performing any experiments. To rinse the tubing and the chambers, use a solution of 2% of SDS. For this purpose, a cycle in the autosampler equipment is program with the steps shown in Table 8.7.

Step	Duration (min)	Speed ($\mu\text{L}/\text{min}$)	Volume (mL)
DI water (1:2)	10	100	1
SDS (1:1)	20	300	6
DI water (1:2)	10	100	1

Table 8.7: Summary of cleaning processes.

Once the equipment is cleaned, it is ready to perform an experiment, a second program in the autosampler is loaded with the parameters shown in Table 8.8.

Step	Duration (min)	Speed ($\mu\text{L}/\text{min}$)	Volume (mL)
Buffer (1:3)	7	100	0.7
Nanoparticles (1:4)	30	100	3.0

Table 8.8: Experimental set-up.

The purpose of flowing the buffer in the beginning is to provide a background signal to take into account when running the samples. Usually a small quantity of the sample is loaded into the sensor at a very slow flow rate in order to let the deposition take place.

8.5.2.5 Data acquisition

Example data obtained with the above parameters is shown in Figure 8.39. The blue squares depict the change in the frequency. As the experiment continues, the frequency decreases as more mass is deposited. On the other hand, shown as the red squares, the dissipation increases, describing the increase of both the height and certain loss of the rigidity in the layer from the top of the sensor. To illustrate the different steps of the experiment, each section has been color coded. The blue part of the data obtained corresponds to the flow of the buffer, while the yellow part corresponds to the deposition equilibrium of the nanoparticles onto the gold surface. After certain length of time equilibrium is reached and there is no further change. Once equilibrium indicates no change for about five minutes, it is safe to say the deposition will not change.

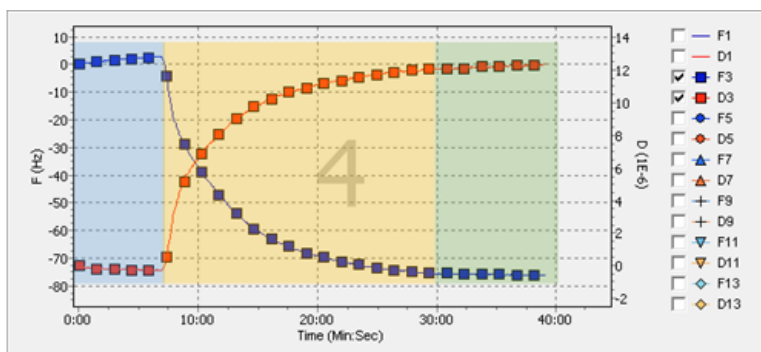


Figure 8.39: Data of deposition of nMag in a gold surface.

8.5.2.6 Instrument clean-up

As a measure preventive care for the equipment, the same cleaning procedure should be followed as what was done before loading the sample. Use of a 2% solution of SDS helps to ensure the equipment remains as clean as possible.

8.5.3 Data modeling

Once the data has been obtained, QTools (software that is available in the software suit of the equipment) can be used to convert the change in the frequency to areal mass, via the Sauerbrey equation, (8.35). The correspondent graph of areal mass is shown in Figure 8.40. From this graph we can observe how the mass is increasing as the nMag is deposited in the surface of the sensor. The blue section again illustrates the part of the experiment where only buffer was been flown to the chamber. The yellow part illustrates the deposition, while the green part shows no change in the mass after a period of time, which indicates the deposition is finished. The conversion from areal mass to mass is a simple process, as gold sensors come with a definite area of 1 cm^2 , but a more accurate measure should be taken when using functionalized sensors.

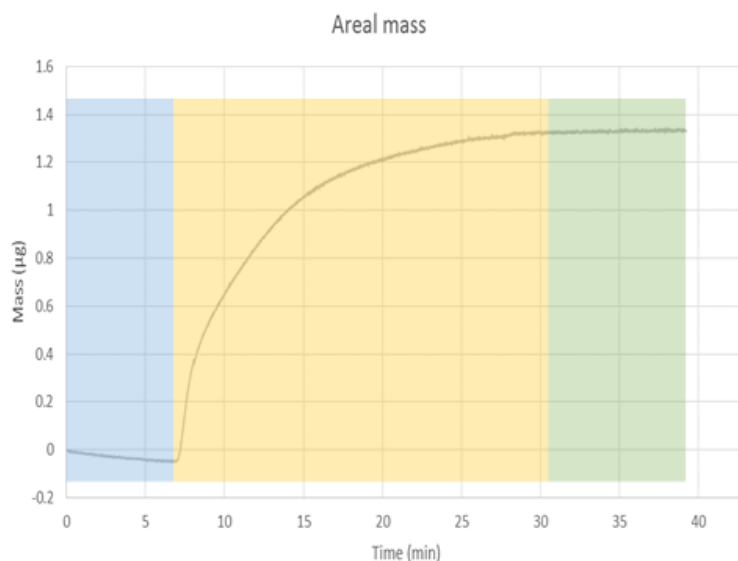


Figure 8.40: Areal mass of deposition of nMag into gold surface.

It is important to take into account the limitations of the Saubery equation, because the equation accounts for a uniform layer on top of the surface of the sensor. Deviations due to clusters of material deposited in one place or the formation of partial multilayers in the sensor cannot be calculated through this model. Further characterization of the surface should be done to have a more accurate model of the phenomena.

8.5.4 Bibliography

- Biolin Scientific, *Cleaning and Immobilization Protocols* (2004).
- F. Hook, *Development of a Novel QCM Technique for Protein Adsorption Studies*, Chalmers University (1997).
- C. Ziez, *Theoretical and Experimental Analysis on Nanoparticle-Nanoparticle and Nanoparticle-Surface Interactions and their Role in Defining their Stability and Mobility*, Rice University (2013).